1521-0103/387/3/252–264$35.00
THE JOURNAL OF PHARMACOLOGY AND EXPERIMENTAL THERAPEUTICS
dx.doi.org/10.1124/jpet.123.001681
J Pharmacol Exp Ther 387:252–264, December 2023

An Integrative Approach to Elucidate Mechanisms Underlying the Pharmacokinetic Goldenseal-Midazolam Interaction: Application of In Vitro Assays and Physiologically Based Pharmacokinetic Models to Understand Clinical Observations[S]

James T. Nguyen, Dan-Dan Tian,[1] Rakshit S. Tanna, Christopher M. Arian, Justina C. Calamia, Allan E. Rettie, Kenneth E. Thummel, and Mary F. Paine

Department of Pharmaceutical Sciences, College of Pharmacy and Pharmaceutical Sciences, Washington State University, Spokane, Washington (J.T.N., D.-D.T., R.S.T., M.F.P.); Department of Pharmaceutics (C.M.A., J.C.C., K.E.T.) and Department of Medicinal Chemistry (A.E.R.), School of Pharmacy, University of Washington, Seattle, Washington; and Center of Excellence for Natural Product Drug Interaction Research, Spokane, Washington (A.E.R, K.E.T., M.F.P.)

Received April 9, 2023; accepted July 6, 2023

ABSTRACT

The natural product goldenseal is a clinical inhibitor of CYP3A activity, as evidenced by a 40%–60% increase in midazolam area under the plasma concentration versus time curve (AUC) after coadministration with goldenseal. The predominant goldenseal alkaloids berberine and (−)-β-hydrastine were previously identified as time-dependent CYP3A inhibitors using human liver microsomes. Whether these alkaloids contribute to the clinical interaction, as well as the primary anatomic site (hepatic vs. intestinal) and mode of CYP3A inhibition (reversible vs. time-dependent), remain uncharacterized. The objective of this study was to mechanistically assess the pharmacokinetic goldenseal-midazolam interaction using an integrated in vitro–in vivo–in silico approach. Using human intestinal microsomes, (−)-β-hydrastine was a more potent time-dependent inhibitor of midazolam 1'-hydroxylation than berberine (K_I and k_{inact}: 8.48 μM and 0.041 minutes^{-1}, respectively, vs. >250 μM and ∼0.06 minutes^{-1}, respectively). Both the AUC and C_{max} of midazolam increased by 40%–60% after acute (single 3-g dose) and chronic (1 g thrice daily × 6 days) goldenseal administration to healthy adults. These increases, coupled with a modest or no increase (≤23%) in half-life, suggested that goldenseal primarily inhibited intestinal CYP3A. A physiologically based pharmacokinetic interaction model incorporating berberine and (−)-β-hydrastine successfully predicted the goldenseal-midazolam interaction to within 20% of that observed after both chronic and acute goldenseal administration. Simulations implicated (−)-β-hydrastine as the major alkaloid precipitating the interaction, primarily via time-dependent inhibition of intestinal CYP3A, after chronic and acute goldenseal exposure. Results highlight the potential interplay between time-dependent and reversible inhibition of intestinal CYP3A as the mechanism underlying natural product-drug interactions, even after acute exposure to the precipitant.

SIGNIFICANCE STATEMENT

Natural products can alter the pharmacokinetics of an object drug, potentially resulting in increased off-target effects or decreased efficacy of the drug. The objective of this work was to evaluate fundamental mechanisms underlying the clinically observed goldenseal-midazolam interaction. Results support the use of an integrated approach involving established in vitro assays, clinical evaluation, and physiologically based pharmacokinetic modeling to elucidate the complex interplay between multiple phytoconstituents and various pharmacokinetic processes driving a drug interaction.

Introduction

The botanical natural product goldenseal [*Hydrastis canadensis* L. (Ranunculaceae)], a perennial herb native to North America, is commonly used to self-treat the common cold and other respiratory infections, allergic rhinitis, and digestive complications such as diarrhea and constipation (Hobbs, 1990) (https://www.nccih.nih.gov/health/goldenseal). Gurley and colleagues previously reported goldenseal to precipitate clinically significant interactions with midazolam, a drug that undergoes extensive metabolism via cytochrome P450 (P450) 3A–mediated hydroxylation (Kronbach et al., 1989; Tian et al., 2019). The metabolic ratio, as determined by the plasma 1'-hydroxymidazolam/midazolam ratio measured at a single blood collection time point, decreased by 40% after a 4-week

This work was supported by the National Institutes of Health National Center for Complementary and Integrative Health (NCCIH) and Office of Dietary Supplements, specifically the Center of Excellence for Natural Product Drug Interaction Research [Grant U54 AT008909] (to M.F.P.) and NCCIH [Grant F31 AT011698] (to J.T.N.). The content is solely the responsibility of the authors and does not necessarily represent the official views of the National Institutes of Health.

M.F.P. is a member of the Scientific Advisory Board for Simcyp, Certara UK Limited.

Part of this work was presented as follows: Nguyen J, Tanna R, Tian D, Arian C, Cech N, Oberlies N, Rettie A, Thummel K, and Paine M (2022) Elucidating mechanisms underlying a pharmacokinetic natural product-drug interaction using a modeling and simulation approach (Abstract). *24th North American ISSX Meeting*; 2022 Sept 11–14; Seattle, WA. International Society for the Study of Xenobiotics, Washington, DC.

[1]Current affiliation: Department of Drug Disposition, Eli Lilly and Company, Indianapolis, Indiana.

dx.doi.org/10.1124/jpet.123.001681.

[S] This article has supplemental material available at jpet.aspetjournals.org.

administration of goldenseal root extract (900 mg thrice daily) to 12 healthy adult participants (Gurley et al., 2005). The decreased CYP3A activity was recapitulated by a 1.6-fold increase in midazolam area under the plasma concentration versus time curve (AUC) after 2 weeks of goldenseal root extract administration (1.3 g thrice daily) to 16 healthy adults (Gurley et al., 2008). These observations clearly indicate that goldenseal is a clinical inhibitor of CYP3A. However, the primary precipitant, mode of inhibition, and site of interaction remain uncharacterized.

Major phytoconstituents of goldenseal include the isoquinoline alkaloids berberine and (−)-β-hydrastine. These alkaloids contain methylenedioxyphenyl moieties, which are known structural alerts for potential time-dependent inhibition (TDI) of P450s (Kalgutkar et al., 2007). Both berberine and (−)-β-hydrastine demonstrated TDI of CYP3A activity (midazolam 1'-hydroxylation) in human liver microsomes (HLMs) (Chatterjee and Franklin, 2003; McDonald et al., 2020). The k_{inact}/K_I ratios for berberine and (−)-β-hydrastine were 1.3 and 2.0 ml/min/μmol, respectively (McDonald et al., 2020). Berberine also activated midazolam 1'-hydroxylation in both HLMs and recombinant CYP3A5, but not recombinant CYP3A4, as shown by a reduction in $K_{m(app)}$. In addition to the liver, the intestine represents a potential site for first-pass drug interactions. Based on the presumed high concentrations of exogenous precipitants at this anatomic site, along with the fact that midazolam undergoes extensive first-pass metabolism (Paine et al., 1996; Thummel et al., 1996), modulation of intestinal CYP3A may contribute to the observed goldenseal-midazolam interaction.

Physiologically based pharmacokinetic (PBPK) modeling is a dynamic tool that can provide mechanistic insights into biologic processes governing an observed pharmacokinetic interaction by integrating organ physiology with compound-dependent physicochemical and pharmacokinetic parameters (Sager et al., 2015). Unlike for drug-drug interactions, the application of PBPK modeling to natural product-drug interactions remains underutilized due to the phytochemical complexity of natural products, the contents of phytoconstituents in marketed products varying between different manufacturers, and the lack of robust physicochemical and pharmacokinetic data for most phytoconstituents. A PBPK model for goldenseal was previously developed and verified to simulate the observed goldenseal-midazolam interaction (Adiwidjaja et al., 2022). Although the model provided a reliable estimate of the magnitude of the interaction, elucidating mechanisms underlying this natural product-drug interaction was not a premise of the study.

The objective of the current study was to elucidate the fundamental mechanism(s) underlying the goldenseal-midazolam interaction using a comprehensive integrated approach involving established in vitro assays, clinical evaluation, and PBPK modeling. The aims were to 1) describe the inhibition kinetics of berberine and (−)-β-hydrastine toward intestinal CYP3A activity using human intestinal microsomes (HIMs), 2) evaluate the pharmacokinetics of midazolam before and after oral administration of a well-characterized goldenseal product to healthy adult participants, and 3) develop a PBPK model to gain further mechanistic insights into the goldenseal-mediated drug interaction (i.e., contributions between reversible inhibition and TDI by berberine and/or (−)-β-hydrastine and the predominant anatomic site of interaction). Results illustrate how this integrated approach can be used to elucidate the complex interplay between multiple phytoconstituents and multiple pharmacokinetic processes driving an observed natural product-drug interaction.

Materials and Methods

Chemicals and Reagents. Midazolam, 1'-hydroxymidazolam, 4-hydroxymidazolam, midazolam 1'-*O*-glucuronide, midazolam 4-*O*-glucuronide, midazolam *N*-glucuronide, alprazolam, β-nicotinamide adenine dinucleotide phosphate (NADPH), ketoconazole, atenolol, berberine chloride, (−)-β-hydrastine (USP reference standard), and penicillin/streptomycin (10,000 units/10 mg per ml) were purchased from Sigma-Aldrich (St. Louis, MO). HIMs (10 mg/ml; H0610.I, lot 1610314), pooled from 15 donors of mixed sex, were purchased from Xenotech (Kansas City, KS). Fasted state simulated intestinal fluid (FaSSIF) was acquired from Biorelevant (London, UK). Caco-2 cells were procured from American Type Culture Collection (ATCC) (Manassas, VA). All other chemicals and reagents were of analytical grade.

IC_{50} Shift Experiment for the Predominant Goldenseal Alkaloids Using HIMs. The primary mixture contained HIMs (0.05 mg/ml), potassium phosphate buffer (100 mM, pH 7.4), and either berberine or (−)-β-hydrastine (0.1–500 μM) incubated in the presence and absence of NADPH (1 mM). After 30 minutes at 37°C, 196 μl of the mixtures were transferred to a secondary reaction, which contained 2 μl midazolam (final concentration: 4 μM) and either 2 μl potassium phosphate buffer or 2 μl NADPH (final concentration: 1 mM). The final methanol concentration in all incubation mixtures was ≤1% (v/v). Reactions were terminated after 10 minutes by removing 100 μl of the mixture and adding to 200 μl of ice-cold methanol containing alprazolam (100 nM) as internal standard. After centrifugation (3800 g × 10 minutes), the supernatant was analyzed for 1'-hydroxymidazolam using ultrahigh-performance liquid chromatography tandem mass spectrometry (UHPLC-MS/MS) (Supplemental Table 1). IC_{50} values were recovered from percent control activity versus log-transformed concentration data via nonlinear regression using GraphPad Prism 9 (GraphPad Software Inc., La Jolla, CA).

Time-Dependent Inhibition of Midazolam 1'-Hydroxylation in HIMs by Goldenseal Alkaloids. HIMs (0.05 mg/ml) diluted in potassium phosphate buffer were incubated with berberine (25–500 μM), (−)-β-hydrastine (3–90 μM), or 6,7-dihydroxybergamottin (1, 0.5 μM); the final concentration of methanol was ≤1% (v/v). Primary incubation mixtures were equilibrated to 37°C, after which the reactions were initiated by adding NADPH (1 mM). After 0, 2, 5, 10, 15, and 20 minutes, 198 μl of the mixture were added to a tube containing 2 μl of midazolam (final concentration: 40 μM). The secondary incubations were terminated 5 minutes later with one volume of ice-cold methanol containing alprazolam (100 nM) as internal standard. After centrifugation (3800 g × 10 minutes), the supernatant was analyzed for 1'-hydroxymidazolam using UHPLC-MS/MS (Supplemental Table 1). K_I and k_{inact} estimates were recovered from $k_{inact,app}$ versus [I] data, which were analyzed via nonlinear regression using Phoenix

ABBREVIATIONS: AUC, area under the plasma concentration versus time curve; AUC_{0-12h}, AUC from 0 to 12 hours; AUC_{inf}, AUC from time zero to infinity; $AUC_{0-tlast}$, AUC from time zero to last measured concentration; Cl/F, oral clearance; CL_R, renal clearance; FaSSIF, fasted state simulated intestinal fluid; HIM, human intestinal microsome; HLM, human liver microsome; P_{app}, apparent permeability; PBPK, physiologically based pharmacokinetic; $t_{1/2}$, terminal half-life; TDI, time-dependent inhibition; t_{max}, time to reach C_{max}; UHPLC-MS/MS, ultrahigh-performance liquid chromatography tandem mass spectrometry.

WinNonlin (v7.0; Certara USA, Princeton, NJ) as described (Brantley et al., 2013; Tanna et al., 2021).

Allosterism of Midazolam Hydroxylation in HIMs by Berberine. HIMs (0.05 mg/ml) diluted in potassium phosphate buffer were incubated with berberine (5–100 μM) and midazolam (0.5–250 μM). Control mixtures contained ≤1% (v/v) methanol in place of berberine. Reactions proceeded for 5 minutes after initiating with NADPH (1 mM). Samples were processed as described above and analyzed for 1'-hydroxymidazolam and 4-hydroxymidazolam using UHPLC-MS/MS (Supplemental Table 1). Relative changes in V_{max} and K_m were visualized from initial velocity versus [S] data.

Dissolution Profiles of the Predominant Goldenseal Alkaloids. The goldenseal product administered to the clinical study participants was extensively characterized as described (Kellogg et al., 2020; Wallace et al., 2020). In brief, each gram of the product (Now Foods, Bloomingdale, IL) contained 29.8 mg of berberine and 25.4 mg of (−)-β-hydrastine. The dissolution profiles for berberine and (−)-β-hydrastine were determined in fasted state simulated intestinal fluid (FaSSIF) using Apparatus 2 (708-DS Dissolution Apparatus; Agilent Technologies, Santa Clara, CA). To mimic the physiologic conditions established in the previously published clinical study (Nguyen et al., 2021), two capsules of the goldenseal product (500 mg/capsule) were added to 250 ml of FaSSIF in glass vessels attached with a paddle rotating at 50 rpm. Samples (~1 ml) of the mixture were collected at 0, 5, 10, 15, 20, 30, 60, and 120 minutes and filtered through Millex hydrophilic PTFE 0.20 μm membrane filters (Merck Millipore Ltd, Tullagreen, Ireland). Samples were diluted 1:500 in methanol containing the internal standard alprazolam (100 nM) prior to UHPLC-MS/MS analysis for berberine and (−)-β-hydrastine (Supplemental Table 1).

Permeability Assessment of Major Goldenseal Alkaloids. The apparent permeability (P_{app}) for berberine and (−)-β-hydrastine (10 μM) was determined using Caco-2 cell monolayers, which were developed with cells of low passage count (12–30) using established methods (Hubatsch et al., 2007). In brief, Caco-2 cells were seeded onto 12-mm Transwell polyester membrane inserts (Corning 3460; Corning, NY) at a density of 3×10^5 cells/cm^2 and grown for 21–28 days in Dulbecco's modified Eagle's medium (Corning 10-009-CV) supplemented with 20% fetal bovine serum (ATCC 30-2020) and penicillin/streptomycin (final concentration: 100 units/0.1 mg/ml). P_{app} in the apical to the basolateral direction was assessed for each test article. P_{app} for berberine, (−)-β-hydrastine, and the low permeability control atenolol (10 μM) was determined after 30 and 60 minutes of incubation, whereas P_{app} for the high permeability control midazolam (10 μM) was determined after 15 and 30 minutes. Samples were diluted in methanol containing alprazolam (100 nM; internal standard) prior to UHPLC-MS/MS analysis (Supplemental Table 1). To ensure the integrity of cell monolayers, only those with a net transepithelial electrical resistance measurement ≥220 were used.

Clinical Pharmacokinetic Goldenseal-Midazolam Interaction Study. The clinical protocol and consent form were approved by the Washington State University (WSU) Institutional Review Board (IRB 16620) and registered in the ClinicalTrials.gov database (NCT03772262). All clinical activities were conducted at the WSU Clinical Research Unit on the Health Sciences Campus in accordance with 45 CFR 46 and adherence to Good Clinical Practice guidelines. The study was initially conducted in an open-label, two-arm (baseline and chronic goldenseal exposure), fixed sequence crossover manner as described (Nguyen et al., 2021). In brief, during the baseline arm, healthy adult participants (eight males, eight females) were orally administered 2.5 mg midazolam syrup (West-Ward Pharmaceuticals, Eatontown, NJ) as a sensitive CYP3A substrate in a probe drug cocktail. After at least a 1-week washout, participants were administered 1 g goldenseal thrice daily for 6 days (chronic exposure). On the sixth day, they were administered the probe drug cocktail containing midazolam ~30 minutes after the first dose of goldenseal. For both arms, plasma and urine were collected up to 96 and 24 hours, respectively, after midazolam administration. A subset of these participants (four males, four females) completed an exploratory study to determine whether a single large dose of goldenseal (acute exposure) would precipitate a pharmacokinetic interaction with midazolam. During this arm, participants were administered a single 3-g dose of goldenseal ~30 minutes prior to midazolam syrup (2.5 mg). Plasma and urine were collected up to 12 hours after midazolam administration in the acute exposure arm. During the three study arms, vital signs (blood pressure, pulse, oxygen saturation) were recorded periodically throughout the inpatient day. Plasma and urine were analyzed for midazolam, midazolam metabolites, berberine, and (−)-β-hydrastine via UHPLC-MS/MS (Supplemental Table 1).

Pharmacokinetic Analysis. The pharmacokinetics of midazolam, midazolam metabolites, berberine, and (−)-β-hydrastine were determined by noncompartmental analysis using Phoenix WinNonlin as described (Tian et al., 2019). The following were recovered: plasma AUC from time zero to the last measured concentration ($AUC_{0-tlast}$), AUC from time zero to infinity (AUC_{inf}), terminal half-life ($t_{1/2}$), maximum plasma concentration (C_{max}), time to reach C_{max} (t_{max}), oral clearance (Cl/F), and renal clearance (CL_R). Midazolam $AUC_{0-tlast}$ was determined up to 12 hours after administration due to concentrations being below the limit of quantification.

Statistical and Power Analysis. The clinical study was initially designed and powered to assess the effects of chronic goldenseal exposure on midazolam pharmacokinetics as previously reported (Nguyen et al., 2021); the protocol was later amended to include the exploratory acute goldenseal exposure arm. The primary endpoints included the chronic goldenseal exposure-to-baseline ratios of midazolam $AUC_{0-tlast}$ and AUC_{inf} with a predefined no effect range of 0.80–1.25. Secondary endpoints included C_{max}, $t_{1/2}$, Cl/F, and CL_R of midazolam after chronic goldenseal exposure; $AUC_{0-tlast}$, AUC_{inf}, C_{max}, $t_{1/2}$, and CL_R of midazolam metabolites after chronic goldenseal exposure; and all of these pharmacokinetic measures for midazolam and metabolites after acute goldenseal exposure. Statistical analyses were performed on all secondary endpoints using Wilcoxon matched-pairs signed-rank test.

PBPK Modeling of the Goldenseal-Midazolam Interaction. The PBPK model was developed using the modeling and simulation platform Simcyp (v22; Certara USA, Princeton, NJ); the model structure has been extensively described elsewhere (Jamei et al., 2009, 2013; Pathak et al., 2017). The default midazolam model within the software was applied to evaluate CYP3A-mediated drug interactions (Supplemental Methods). The inhibitor models for berberine and (−)-β-hydrastine were developed using physicochemical properties, in vitro–derived kinetic parameters, and external pharmacokinetic data (Supplemental Table 2) and verified with the current clinical pharmacokinetic study. Based on the dissolution and permeability results, the first-order absorption model was selected for the berberine PBPK model, whereas the advanced dissolution, absorption, and metabolism (ADAM) model was adapted for the (−)-β-hydrastine PBPK model. Due to limitations of the modeling and simulation platform, only one inhibition value (obtained from either HIMs or HLMs) can be used to characterize the interaction potential for a given inhibitor; thus, the value correlating with the highest inhibition potency was used for model development. Simulations were conducted in a virtual population with demographics matching those of the participants enrolled in the current clinical study (Supplemental Table 3). Model predictions were considered successful if the predicted $AUC_{0-tlast}$ and C_{max} were within 2-fold of observed values.

Results

IC_{50} Shift for Berberine and (−)-β-Hydrastine in HIMs. An IC_{50} shift for berberine was not observed due to apparent activation of midazolam 1'-hydroxylation in the absence of NADPH in the primary incubation (Fig. 1A). In contrast, an ~15-fold leftward shift in IC_{50} was observed for (−)-β-hydrastine after preincubation with NADPH (Fig. 1B).

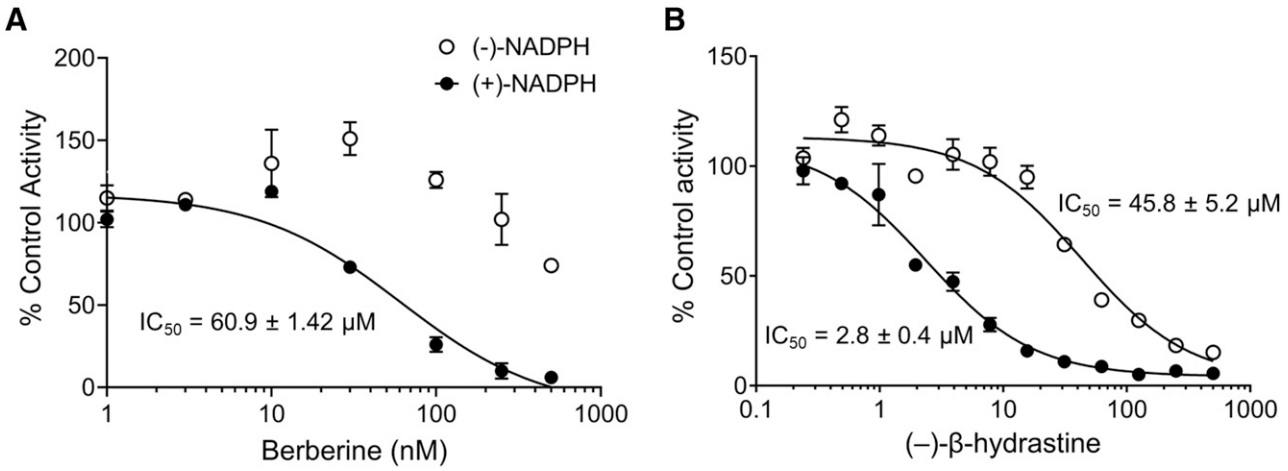

Fig. 1. IC_{50} for berberine (A) and (−)-β-hydrastine (B) preincubated with human intestinal microsomes in the presence and absence of NADPH. The index reaction, midazolam 1'-hydroxylation (4 μM midazolam), was used to assess CYP3A activity. Symbols and error bars denote means and standard deviations, respectively, of triplicate incubations. Lines denote nonlinear least-squares regression of the percent control activity versus log-transformed concentration data.

Time-Dependent Inhibition of Midazolam 1'-Hydroxylation by Berberine and (−)-β-Hydrastine in HIMs. Both berberine and (−)-β-hydrastine exhibited concentration-dependent and time-dependent inhibition of midazolam 1'-hydroxylation (Fig. 2). K_I, k_{inact}, and k_{inact}/K_I for (−)-β-hydrastine were 8.48 ± 3.09 μM, 0.041 ± 0.0034 minutes^{-1}, and 4.83 ml/min/μmol, respectively. A robust estimate of K_I and k_{inact} for berberine could not be obtained because testing concentrations higher than 500 μM exceeded the solubility limit. As such, the maximum $k_{inact,app}$ (0.061 ± 0.001 minutes^{-1}) was used as a conservative estimate of k_{inact}, of which the corresponding K_I was 250 μM. Using

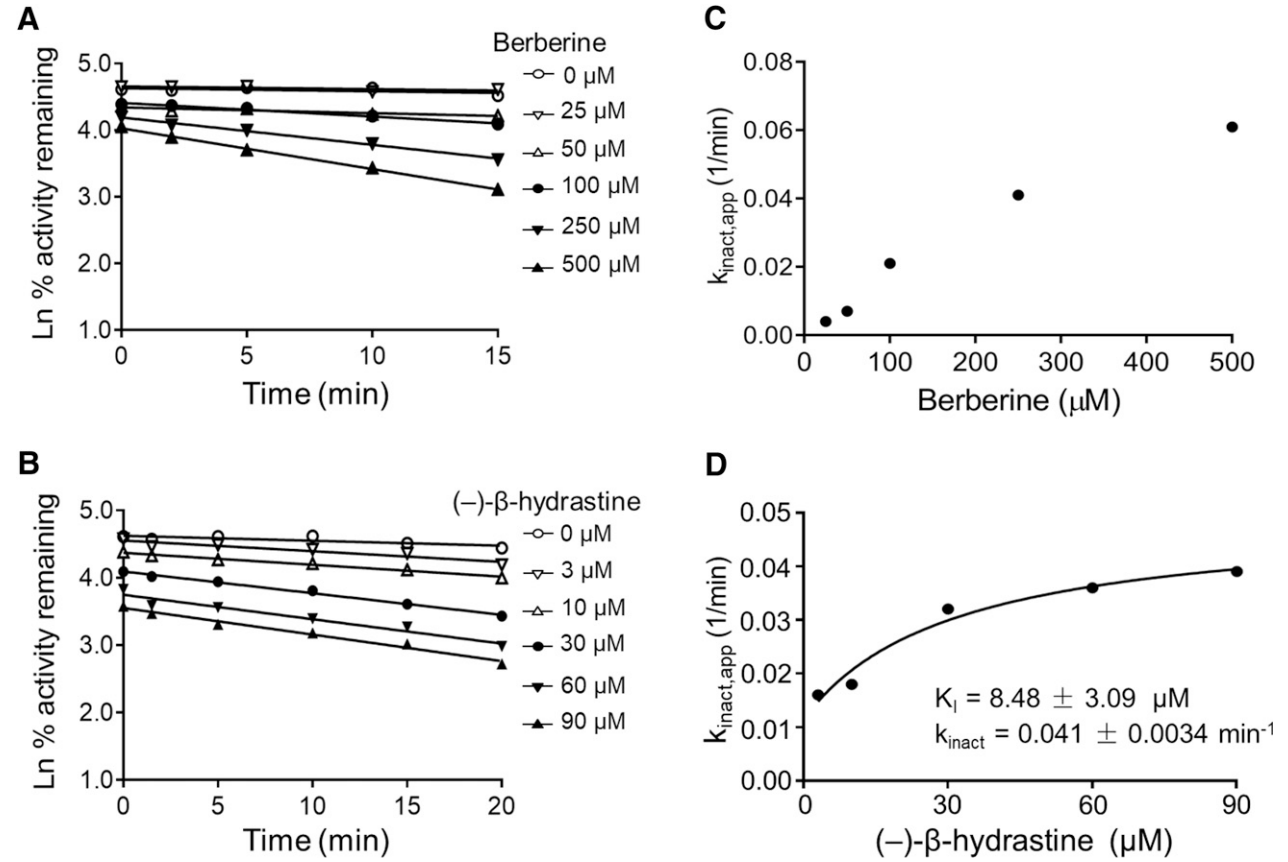

Fig. 2. Time-dependent inhibitory effects of berberine (A) and (−)-β-hydrastine (B) on midazolam 1'-hydroxylation in human intestinal microsomes. Symbols and lines denote means of duplicate incubations and linear regression of initial monoexponential decline in activity, respectively. Corresponding graphs on the right (C and D) depict the rate of CYP3A inactivation as a function of inhibitor concentration. Symbols denote observed inactivation rates at each inhibitor concentration, and the curve (D) denotes nonlinear least-squares regression of the observed data. A robust estimate of K_I and k_{inact} for berberine (C) could not be recovered because testing concentrations higher than 500 μM exceeded the solubility limit.

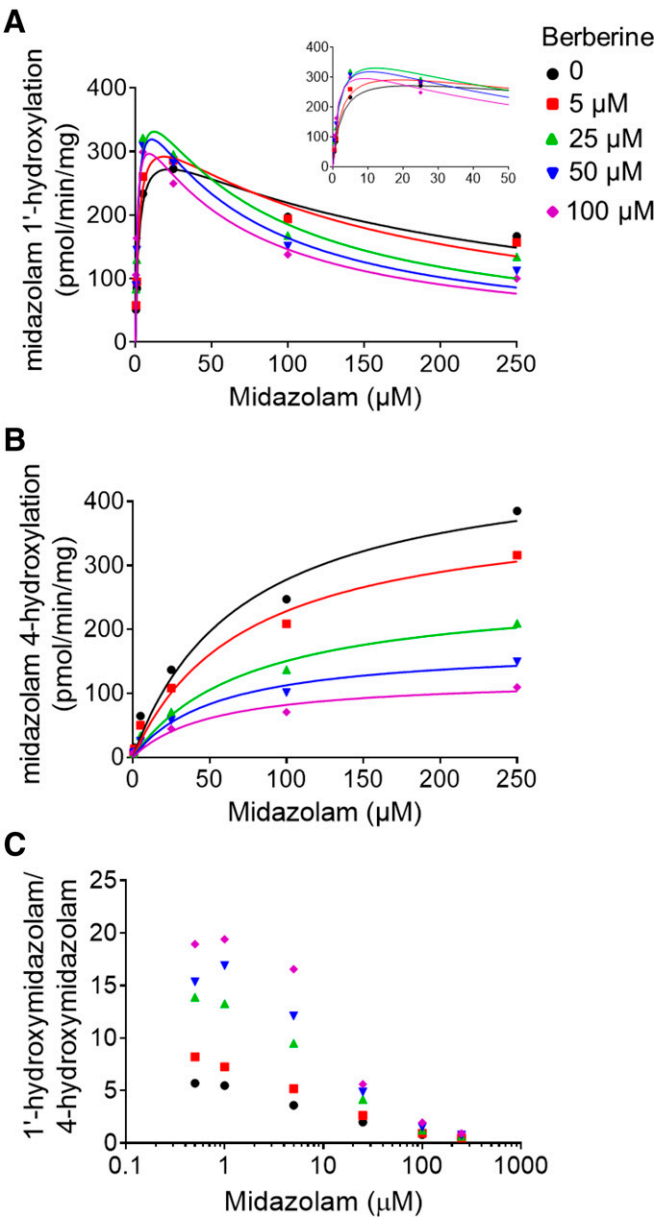

Fig. 3. Effects of berberine (5–100 μM) on the rate of midazolam 1'-hydroxylation (A) and 4-hydroxylation (B) in human intestinal microsomes at midazolam concentrations ranging from 5 to 250 μM. The corresponding ratios of 1'-hydroxymidazolam to 4-hydroxymidazolam (C) are shown for midazolam concentrations up to 250 μM.

these values, k_{inact}/K_I for berberine was estimated to be 0.244 ml/min/μmol.

Allosterism of Midazolam Hydroxylation by Berberine in HIMs. Using a reversible inhibition experimental design, berberine activated 1'-hydroxymidazolam formation at midazolam concentrations $\leq$5 μM but inhibited the reaction at concentrations $\geq$50 μM (Fig. 3A). In contrast, berberine inhibited midazolam 4-hydroxylation throughout the tested concentration range (5–100 μM) (Fig. 3B). The 1'-hydroxymidazolam/4-hydroxymidazolam ratio decreased with increasing midazolam concentrations (Fig. 3C). Berberine showed a concentration-dependent increase in this ratio, particularly at lower midazolam concentrations ($\leq$5 μM).

Dissolution and Permeability of Berberine and (−)-β-Hydrastine. More than 80% of total berberine and (−)-β-hydrastine content (29.8 and 25.4 mg, respectively) in two goldenseal capsules dissolved in FaSSIF within 20 minutes (Fig. 4, A and B). The P_{app} for berberine and (−)-β-hydrastine was 0.18×10^{-6} and 9.72×10^{-6} cm/s, respectively (Fig. 4C).

Effects of Goldenseal on the Pharmacokinetics of Midazolam and Its Metabolites in Healthy Adult Participants. Midazolam pharmacokinetics observed in the baseline and chronic goldenseal exposure arms have been previously reported (Nguyen et al., 2021). Acute administration of goldenseal resulted in similar changes to midazolam pharmacokinetics as those after chronic administration, albeit the acute goldenseal exposure arm involved only eight of the 16 participants from the baseline/chronic arm (Fig. 5). The geometric mean ratio of midazolam AUC_{0-12h} (AUC from 0 to 12 hours), AUC_{inf}, and C_{max} increased after chronic (30%–40%) and acute (40%–60%) administration (Table 1). Chronic, but not acute, administration modestly increased midazolam half-life. Goldenseal had minimal to no effects on midazolam t_{max} and renal clearance after both chronic and acute administration.

The effects of goldenseal on the pharmacokinetics of midazolam metabolites varied between chronic and acute administration (Table 1). Acute goldenseal increased the AUC of 1'-hydroxymidazolam, leading to no change in the metabolite-to-parent AUC ratio, whereas chronic goldenseal had no effect on the AUC of 1'-hydroxymidazolam, leading to a decrease in the metabolite-to-parent AUC ratio. Both chronic and acute goldenseal had no effect on the renal clearance of 1'-hydroxymidazolam. Acute goldenseal decreased the C_{max} and metabolite-to-parent AUC ratio of midazolam 1'-*O*-glucuronide, whereas chronic goldenseal only decreased the midazolam 1'-*O*-glucuronide metabolite-to-parent AUC ratio. Chronic and acute goldenseal had variable effects on the minor metabolites 4-hydroxymidazolam, midazolam 4-*O*-glucuronide, and midazolam *N*-glucuronide. The change in midazolam pharmacokinetics after chronic goldenseal exposure for the eight participants who completed all three arms of the study (Supplemental Table 4) was comparable to the change after acute exposure.

***CYP3A5* Genotype.** The demographics of the participants in the clinical study are summarized (Supplemental Table 3). Of the 16 participants who completed the study, 14 were *CYP3A5*3*3* homozygotes, one a *CYP3A5*1*1* homozygote, and one a *CYP3A5*1*3* heterozygote. Because none of the participants carried the nonfunctional variants *CYP3A5*6* and *CYP3A5*7*, a subanalysis of the pharmacokinetic data was not necessary.

PBPK Modeling and Simulation of the Goldenseal-Midazolam Interaction. The developed PBPK models predicted the $AUC_{0-12.5h}$ and C_{max} of berberine and (−)-β-hydrastine to within 2-fold of those observed after a single dose and multiple doses of goldenseal (Table 2). In addition, the simulated plasma concentration-time profiles for berberine and (−)-β-hydrastine accurately described the concentrations observed after chronic and acute goldenseal exposure in healthy adult participants (Fig. 6). However, the extrapolated area ($AUC_{tlast-inf}$) for the observed berberine AUC_{inf} exceeded 20% of $AUC_{0-tlast}$, resulting in an underprediction of AUC_{inf} (Table 2) due to lack of a robust estimate of the terminal half-life in model simulations.

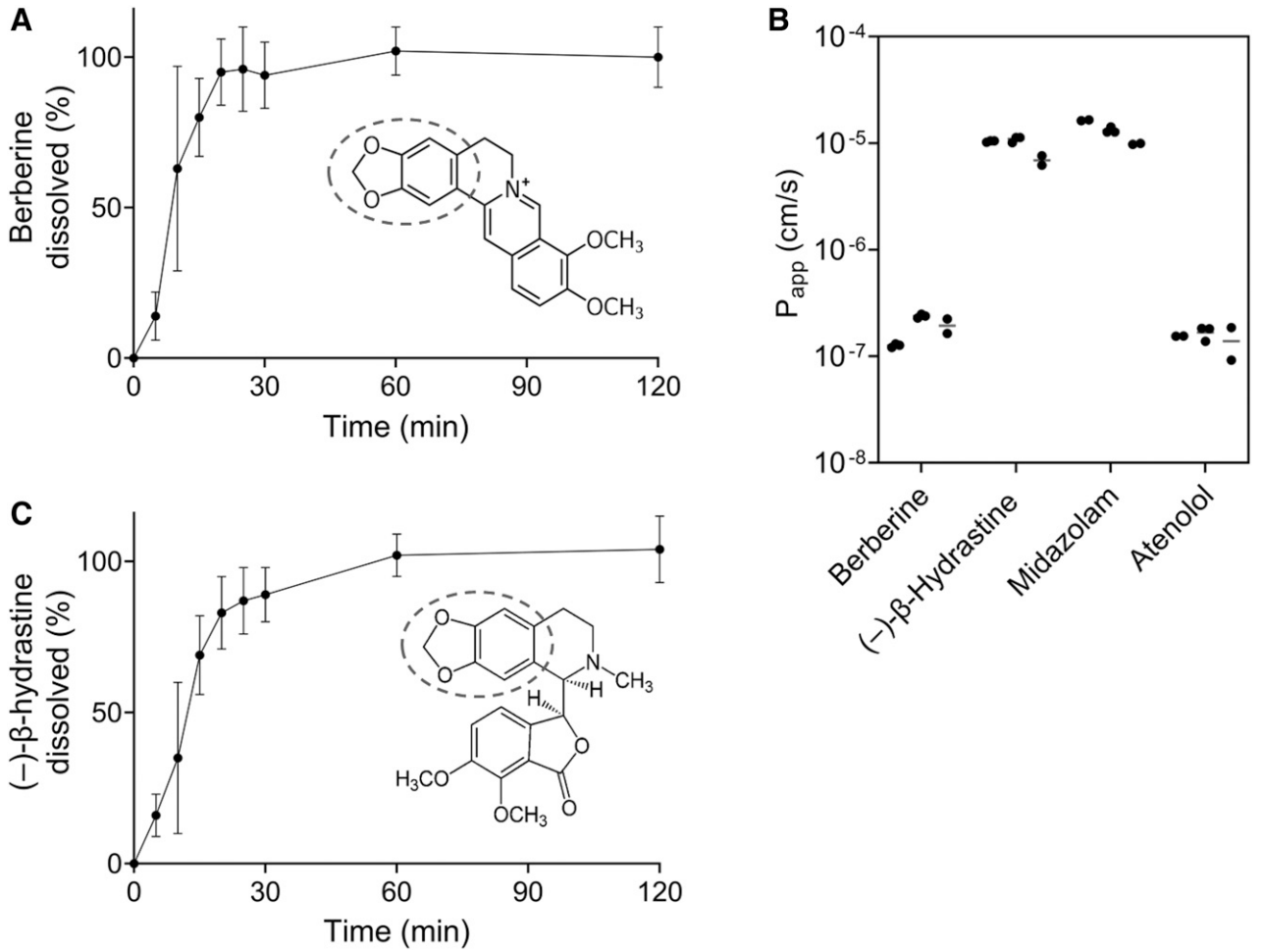

Fig. 4. Dissolution profiles for berberine (A) and (−)-β-hydrastine (B) observed in FaSSIF over the course of 2 hours and apical-to-basolateral translocation (C) of berberine and (−)-β-hydrastine in Caco-2 cell monolayers grown on Transwell inserts. Midazolam and atenolol served as high and low permeability controls, respectively. Symbols and error bars denote means and standard deviations, respectively, of three replicates (A and B); areas circled by dashes represent the methylenedioxyphenyl moiety, a structural alert for time-dependent inhibition. Horizontal lines (C) denote means of two to three replicates from three separate experiments.

Simulations using the midazolam PBPK model in conjunction with the berberine and (−)-β-hydrastine models resulted in predicted pharmacokinetic interactions that were within 1.2-fold of those observed after chronic (Fig. 7A) and acute (Fig. 7B) goldenseal administration (Table 3). Simulations of active CYP3A enzyme after chronic (Fig. 7C) and acute (Fig. 7D) goldenseal administration showed that goldenseal primarily inhibited CYP3A in the small intestine, with maximum inhibition occurring at ~2 hours after administration of the precipitant. In addition, modeling and simulations indicated that the drug interaction risk (as determined by midazolam AUC ratio >1.25) is sustained for ~24 hours after goldenseal exposure (Fig. 7, E and F). Simulations with intravenously administered midazolam resulted in no drug interactions (Supplemental Table 5); similarly, no interactions were predicted when either the (−)-β-hydrastine model or time-dependent inhibition component was removed from the simulations.

Discussion

Natural product-drug interactions remain a longstanding public health concern as more patients seek natural alternatives to supplement their pharmacotherapeutic regimens (Johnson et al., 2018; Safari et al., 2022). Goldenseal is one natural product that has been shown to inhibit CYP3A activity in humans. However, the major precipitant(s), mode of inhibition, and site of the interaction remain largely unknown. Three aspects of the pharmacokinetic goldenseal-midazolam interaction were evaluated: berberine versus (−)-β-hydrastine, reversible inhibition versus TDI, and gut versus liver. Physicochemical, CYP3A inhibition kinetic, and clinical pharmacokinetic data were used to develop a robust PBPK interaction model. Results from this integrated approach indicated that (−)-β-hydrastine, TDI of CYP3A, and the intestine are the predominant precipitant, mechanism, and site of the interaction.

The abundant goldenseal alkaloids berberine and (−)-β-hydrastine were selected as potential precipitants of the pharmacokinetic goldenseal-midazolam interaction because both contain a methylenedioxyphenyl functional group (Fig. 4), a structural moiety associated with TDI (Kalgutkar et al., 2007). The CYP3A inhibition kinetics for both alkaloids were previously established using HLMs (McDonald et al., 2020). Because the parameters obtained from HLMs can vary from those obtained from HIMs (Lalovic et al., 2004), additional in vitro experiments were conducted. Regarding reversible inhibition, effects of a given alkaloid were consistent between

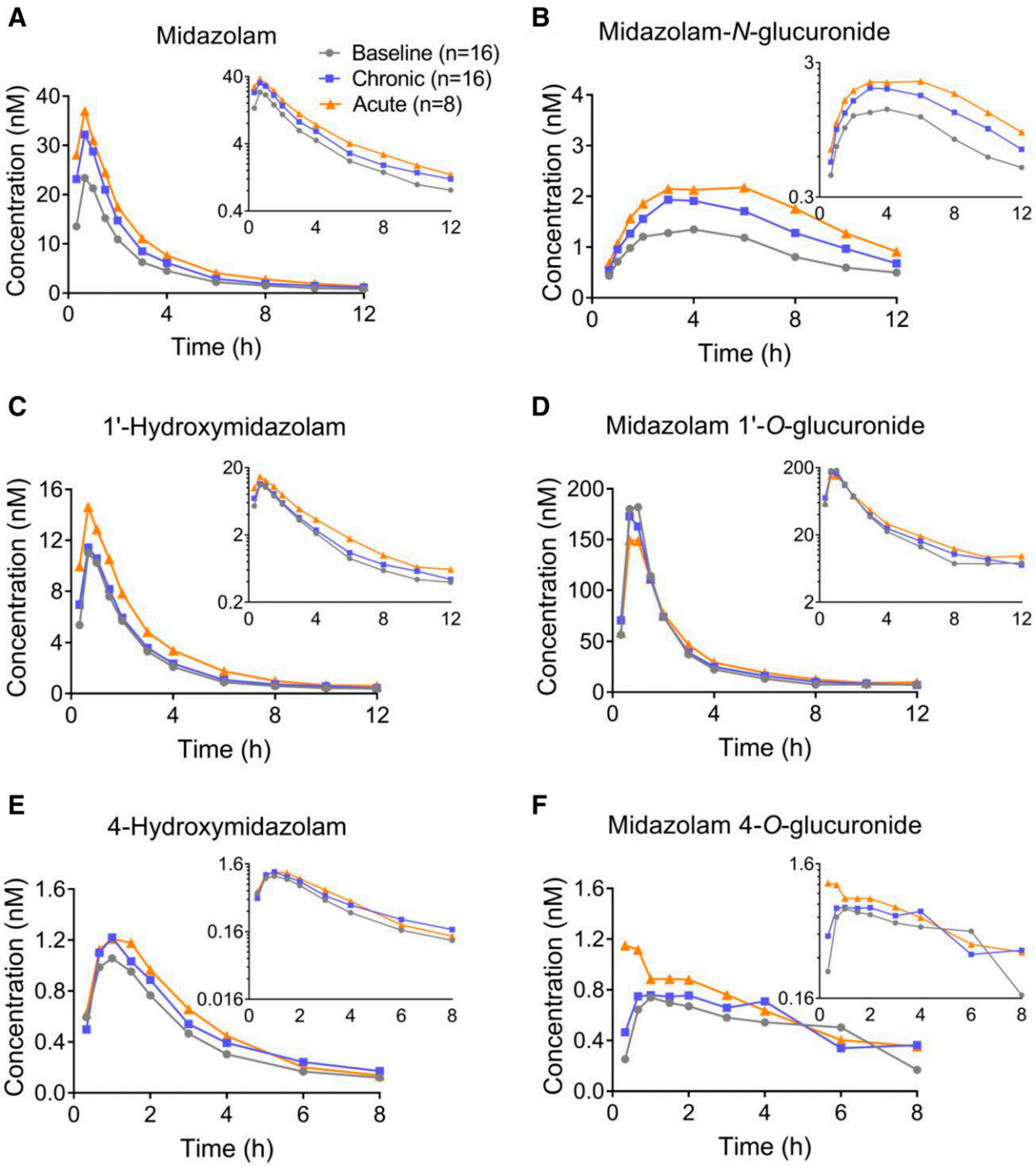

Fig. 5. Plasma concentration-time profiles for midazolam (A), midazolam-*N*-glucuronide (B), 1'-hydroxymidazolam (C), midazolam 1'-*O*-glucuronide (D), 4-hydroxymidazolam (E), and midazolam 4-*O*-glucuronide (F) after oral administration of a single dose of midazolam (2.5 mg) to healthy adult participants in the absence of goldenseal (gray) and after chronic (blue) and acute (orange) exposure to goldenseal. Symbols denote geometric means of the indicated number of participants except for midazolam 4-*O*-glucuronide, which represents arithmetic means of two participants. Error bars are excluded for visual clarity; the reader is referred to Table 1 for the 90% confidence intervals of various pharmacokinetic parameters. The profiles for midazolam at baseline and after chronic goldenseal administration (A) are reprinted with permission from the American Society for Clinical Pharmacology and Therapeutics from Nguyen et al. (2021).

HIMs and HLMs. That is, the IC_{50} for berberine was unattainable from both enzyme sources (due to solubility limitations when >500 μM), and the IC_{50} for (−)-β-hydrastine was comparable (46 vs. 58 μM in HIMs and HLMs, respectively). However, regarding TDI, the inactivation efficiency (k_{inact}/K_I) for berberine in HIMs was estimated to be 5× lower than that in HLMs (~0.24 vs. 1.3 ml/min/μmol), whereas the k_{inact}/K_I for (−)-β-hydrastine in HIMs was moderately higher than that in HLMs (4.8 vs. 2.0 ml/min/μmol) (McDonald et al., 2020). These discrepancies may be attributed to differences in CYP3A4/5 structure, modulation, and/or expression between HIMs and HLMs (Lin et al., 2002), as well as differences in the protein

TABLE 1

Pharmacokinetics of midazolam and its metabolites after oral administration of midazolam (2.5 mg) alone and after chronic (1 g thrice daily for 6 days) or acute (a single dose of 3 g) exposure to goldenseal
Data represent geometric means [90% confidence intervals].

	Baseline (n = 16)	Chronic Exposure (n = 16)	Acute Exposure (n = 8)
Midazolam (MDZ)[a]			
AUC_{0-12h} (nM*h)	61.7 [50.8–74.9]	85.8 [69.3–106.4][b]	101.5 [81.7–126.1]*
AUC_{inf} (nM*h)	67.1 [54.6–82.5]	96.2 [77.0–120.2][b]	112.6 [87.1–145.4]*
$t_{1/2}$ (h)	3.94 [3.35–4.63]	4.84 [4.19–5.60]*	4.19 [3.24–5.44]
C_{max} (nM)	26.2 [21.7–31.7]	34.5 [27.8–42.7]*	37.5 [29.1–48.3]*
t_{max} (h)[c]	0.67 [0.33–1.00]	0.67 [0.33–1.50]	0.67 [0.33–1.0]
Cl/F (l/h)	114.6 [93.1–140.9]	80.0 [64.2–99.8]*	68.3 [53.0–88.0]*
CL_R (l/h)	0.054 [0.039–0.072]	0.067 [0.052–0.086]*	0.065 [0.040–0.104]
	n = 15		n = 7
MDZ *N*-Glucuronide			
AUC_{0-12h} (nM*h)	10.8 [8.87–13.0]	15.9 [12.9–19.3]*	16.1 [10.8–24.0]
AUC_{inf} (nM*h)	14.0 [11.7–16.7]	23.8 [18.8–30.1]*	24.5 [16.9–35.2]*
$t_{1/2}$ (h)	4.47 [3.96–5.03]	4.86 [4.14–5.69]	4.65 [3.52–6.11]
		n = 15	
C_{max} (nM)	1.44 [1.18–1.75]	2.06 [1.67–2.54]*	2.49 [1.84–3.36]*
t_{max} (h)[c]	4.0 [1.0–6.0]	4.0 [1.0–4.0]	3.5 [0.3–4.0]
MP ratio[d]	0.17 [0.14–0.21]	0.18 [0.14–0.22]	0.16 [0.97–0.25]
CL_R (l/h)	6.57 [5.53–7.79]	6.21 [5.30–7.26]	6.82 [4.81–9.65]
1'-Hydroxymidazolam			
AUC_{0-12h} (nM*h)	29.0 [24.4–34.4]	31.1 [25.8–37.4]	42.1 [32.9–53.7]*
AUC_{inf} (nM*h)	33.1 [27.9–39.0]	35.0 [29.2–41.8]	47.6 [37.8–59.7]*
$t_{1/2}$ (h)	6.25 [5.27–7.40]	4.75 [3.78–5.95]	5.12 [3.69–7.08]
C_{max} (nM)	12.3 [10.2–14.7]	11.7 [9.7–14.0]	15.1 [11.3–20.0]
t_{max} (h)[c]	0.67 [0.33–1.00]	0.67 [0.33–1.50]	0.67 [0.33v1.00]
MP ratio[d]	0.47 [0.40–0.54]	0.36 [0.30–0.42]*	0.41 [0.30–0.55]
CL_R (l/h)	0.17 [0.14–0.20]	0.15 [0.12–0.18]	0.11 [0.08–0.15]
	n = 15		n = 7
MDZ 1'-*O*-Glucuronide			
AUC_{0-12h} (nM*h)	412 [376–450]	418 [382–457]	426 [360–504]
AUC_{inf} (nM*h)	478 [436–524]	490 [446–538]	526 [424–652]
$t_{1/2}$ (h)	5.73 [5.15–6.37]	5.68 [4.80–6.72]	6.58 [5.06–8.55]
C_{max} (nM)	205 [182–230]	185 [166–204]	160 [134–189]*
t_{max} (h)[c]	0.67 [0.67–1.0]	0.67 [0.67–1.5]	1.0 [0.67–1.0]
MP ratio[d]	6.66 [5.50–8.06]	4.87 [3.98–5.94]*	4.20 [3.19–5.51]*
CL_R (l/h)	11.2 [9.3–13.3]	11.4 [10.3–12.6]	10.2 [8.4–12.2]
4-Hydroxymidazolam			
AUC_{0-12h} (nM*h)	2.78 [2.34–3.28]	3.36 [2.81–4.01]*	4.25 [3.46–5.20]*
AUC_{inf} (nM*h)	3.41 [2.98–3.89]	4.14 [3.59–4.76]*	4.70 [3.90–5.66]*
$t_{1/2}$ (h)	1.68 [1.54–1.81]	1.86 [1.58–2.17]	2.20 [1.72–2.80]*
C_{max} (nM)	1.14 [1.00–1.30]	1.26 [1.10–1.44]	1.30 [1.04–1.62]
t_{max} (h)[c]	1.00 [0.67–1.50]	1.00 [0.67–1.50]	1.25 [0.67–1.50]
MP ratio[d]	0.045 [0.039–0.051]	0.039 [0.034–0.044]*	0.042 [0.036–0.048]*
CL_R (l/h)	Concentrations of metabolites in urine were below the detectable limit		
MDZ 4-*O*-Glucuronide[e,f]			
AUC_{0-12h} (nM*h)	12.8[9.4–17.3]	24.5 [18.1–33.1]*	32.9, 42.9
AUC_{inf} (nM*h)	24.2[19.0–30.7]	47.5 [27.6–81.8]*	41.7, 49.2
$t_{1/2}$ (h)	4.27 [2.95–6.14]	6.58 [3.68–11.76]	4.18, 1.97
C_{max} (nM)	3.24 [2.68–3.92]	4.31 [3.69–5.03]*	6.19, 14.1
t_{max} (h)[c]	1.50 [0.67–3.00]	1.75 [1.00-3.00]	2, 0.33
MP ratio[d]	0.21 [0.15–0.30]	0.29 [0.20–0.40]	0.44, 0.32
CL_R (l/h)	Concentrations of metabolites in urine were below the detectable limit		

Cl/F, apparent oral clearance; MP, metabolite-to-parent.
[a]Midazolam pharmacokinetics for the baseline and chronic exposure arms have been previously reported (Nguyen et al., 2021).
[b]Significant differences compared with the baseline arm as determined by predefined no effect range of 0.80–1.25.
[c]Denotes median [range].
[d]Calculated as the ratio of metabolite AUC0–12h to midazolam AUC0–12h.
[e]Pharmacokinetics reported for 10 participants for baseline and chronic exposure. Individual data reported for two participants for acute exposure.
[f]Statistical analysis was not conducted for the MDZ 4-*O*-glucuronide acute exposure group due to the limited sample size.
*$P < 0.05$ when compared with the baseline arm using Wilcoxon matched-pairs signed-rank test.

milieu. Regardless, comparing the recovered k_{inact}/K_I values with clinically relevant time-dependent inhibitors (diltiazem and erythromycin: 2.7 and 3.6 ml/min/μmol, respectively) (Obach et al., 2007), these in vitro observations suggest that (−)-β-hydrastine is the primary alkaloid contributing to the goldenseal-midazolam interaction via TDI.

In addition to the clinical studies conducted by Gurley and colleagues, our group recently completed a pharmacokinetic goldenseal-drug interaction study that included midazolam (Nguyen et al., 2021). Results demonstrated that multiple dose administration of goldenseal for a shorter duration than previous studies led to a comparable increase in midazolam AUC (~40%). One prior study (Gurley et al., 2008) showed a larger increase in midazolam half-life in the presence of goldenseal relative to baseline (3.1 vs. 2.0 hours) compared with our study (4.8 vs. 3.9 hours). This discrepancy is likely due to

TABLE 2
Predicted and observed pharmacokinetics for berberine and (−)-β-hydrastine
Data represent geometric mean [90% confidence intervals].

	Observed	Predicted	Predicted/Observed
	Berberine Pharmacokinetics		
Chronic Goldenseal Exposure[a,b]			
$AUC_{0–12.5h}$ (nM*h)	7.81 [6.17–9.89]	6.75 [6.22–7.32]	0.86
$AUC_{0–24.5h}$ (nM*h)	13.8 [10.7–17.9]	10.3 [9.5–11.2]	0.74
AUC_{inf} (nM*h)[c]	46.7 [36.9–58.9][d]	11.5 [10.6–12.5]	0.24
C_{max} (nM)[e]	0.73 [0.56–0.95]	0.42 [0.39–0.46]	0.58
Acute Goldenseal Exposure[f]			
$AUC_{0–12.5h}$(nM*h)	4.58 [2.93–7.14]	7.75 [7.13–8.41]	1.69
AUC_{inf} (nM*h)[b]	Not determined[g]		
C_{max} (nM)[e]	1.12 [0.63–2.00]	0.95 [0.87–1.03]	0.85
	(−)-β-Hydrastine Pharmacokinetics		
Chronic Goldenseal Exposure[a,b]			
$AUC_{0–12.5h}$ (nM*h)	1258 [926–1709]	1613 [1460–1782]	1.28
$AUC_{0–24.5h}$ (nM*h)	1751 [1296–2365]	1725 [1555–1914]	0.98
AUC_{inf} (nM*h)[c]	1803 [1329–2444]	1732 [1560–1923]	0.96
C_{max} (nM)[e]	236 [168-331]	296 [272-321]	1.25
Acute Goldenseal Exposure[f]			
$AUC_{0–12.5h}$ (nM*h)	1528 [954–2449]	1697 [1533–1880]	1.11
AUC_{inf} (nM*h)[c]	1603 [985–2609]	1728 [1557–1917]	1.07
C_{max} (nM)[e]	677 [415–1104]	886 [817–961]	1.30

[a]Goldenseal (1 g) was administered thrice daily × 6 days. Plasma collection began 30 minutes after the first dose of goldenseal. Each gram of goldenseal product contained 29.8 mg berberine and 25.4 mg (−)-β-hydrastine.
[b]AUCs determined after administration of the first dose of goldenseal on day 6.
[c]Calculated using the terminal slope corresponding to the half-life and extrapolated to time infinity after the final observed concentration for each plasma concentration-time profile.
[d]Extrapolated area from the last measurable timepoint to infinity ($AUC_{tlast–inf}$) exceeded 20%, which is the acceptable threshold for robust AUC_{inf} extrapolations.
[e]Recovered during the first 4 hours immediately after administration of the first dose of goldenseal on day 6.
[f]A single dose of goldenseal (3 g) was administered. Plasma collection began 30 minutes later.
[g]Unable to obtain a robust estimate of terminal slope due to a truncated collection interval.

differences in blood collection intervals (6 vs. 12 hours), with the longer sampling duration providing a more robust estimate of half-life. The current work further showed that a single dose of goldenseal increased midazolam AUC and C_{max} but had no effect on half-life (Table 1). Collectively, results suggest that goldenseal inhibited CYP3A primarily in the gut, consistent with a previous report involving weak CYP3A inhibitors (exposure-to-baseline AUC ratio <2) (Yamada et al., 2020).

To gain additional mechanistic insights into the goldenseal-midazolam interaction, a PBPK interaction model was developed using a middle-out approach, incorporating both in vitro and clinical pharmacokinetic data. PBPK models were developed for berberine and (−)-β-hydrastine independently, which were then used in combination with midazolam to simulate systemic exposure to the two major goldenseal alkaloids and to predict the goldenseal-midazolam interaction. Using a learn-and-confirm method, the first-order absorption model was selected for berberine because absorption is permeability-limited. In contrast, the ADAM model was selected for (−)-β-hydrastine because absorption may be dissolution rate-limited based on its relatively high P_{app}. The resulting PBPK models successfully simulated exposure ($AUC_{0–12.5h}$ and C_{max}) to berberine and (−)-β-hydrastine to within 2-fold of that observed after chronic and acute goldenseal administration (Table 2). However, AUC_{inf} for berberine after chronic goldenseal exposure was underpredicted due to lack of robust estimates of terminal half-life (Fig. 6A). Because the inhibition kinetics of each alkaloid varied between HIMs and HLMs, the K_I and k_{inact} values correlating with the highest recovered k_{inact}/K_I and the lowest reversible K_i values were applied to simulate worst-case interaction scenarios (i.e., highest midazolam AUC ratio). The predicted interactions ($AUC_{0–12h}$ and C_{max} ratios) were within 1.2-fold of those observed after chronic and acute goldenseal administration (Table 3), indicating successful model predictions.

Modeling and simulations revealed that active intestinal and hepatic CYP3A decreased by 60%–80% and 3%–10%, respectively, in the presence of goldenseal (Fig. 7, C and D). Simulation of the interaction using intravenous midazolam resulted in no change in AUC (Supplemental Table 5), supporting the inference that goldenseal inhibits CYP3A primarily in the gut. This observation aligns with results from a previous clinical study in which goldenseal had no effect on the pharmacokinetics of indinavir, a drug primarily metabolized by hepatic CYP3A (Chiba et al., 1997; Sandhu et al., 2003).

PBPK modeling and simulations also implicated (−)-β-hydrastine as the primary precipitant of the goldenseal-midazolam interaction via TDI. Removing either the (−)-β-hydrastine model or TDI from simulations resulted in a <5% decrease in active CYP3A enzyme in the gut/liver and no change in midazolam AUC (Supplemental Table 5). Despite evidence supporting (−)-β-hydrastine as the phytoconstituent precipitating the goldenseal-midazolam interaction, a berberine-mediated pharmacokinetic interaction with midazolam (40% increase in AUC) has been reported (Guo et al., 2012); however, participants in the study were administered a higher dose of berberine (300 mg thrice daily × 14 days). Simulations using the developed PBPK interaction model, adjusted for berberine as the sole inhibitor and dosed in a similar manner as the study referenced, resulted in consistent changes in midazolam pharmacokinetics to those reported (Supplemental Table 5). These results demonstrate that weak inhibitors in natural products could elicit clinically relevant pharmacokinetic interactions because of the high phytoconstituent content commonly found in these products.

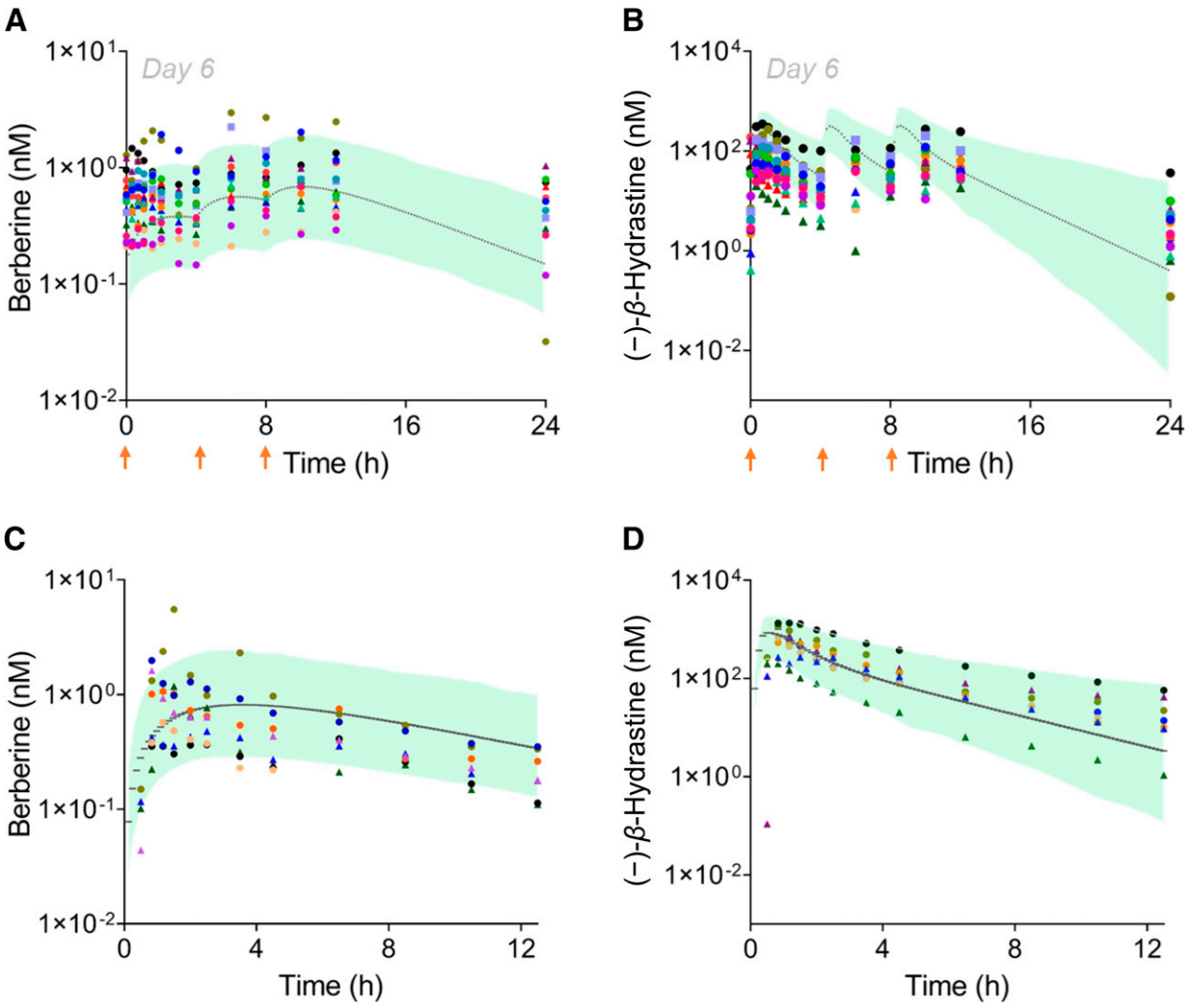

Fig. 6. Observed (colored circles and triangles) and simulated (gray lines) plasma concentration-time profiles for berberine (A and C) and (−)-β-hydrastine (B and D) after oral administration of multiple doses (1 g thrice daily × 6 days) of goldenseal to 16 healthy adult participants (A and B) or a single dose of goldenseal (3 g) to eight healthy adult participants (C and D). Plasma collection for the chronic goldenseal exposure arm (A and B) began after the first dose of goldenseal was administered on day 6; goldenseal administrations are indicated with orange arrows. Each unique symbol-color pair represents a single participant, whereas green-shaded regions denote fifth and 95th percentiles for model simulations. Each gram of the goldenseal product contained 29.8 mg berberine and 25.4 mg (−)-β-hydrastine.

Due to the complexity of characterizing natural product-drug interactions, there are limitations to the current work. First, natural products contain dozens of phytoconstituents that may contribute to an observed interaction. A goldenseal extract, prepared from the product used in the clinical study, showed strong reversible CYP3A inhibition (Supplemental Fig. 1) that was not observed with the two primary alkaloids. Accordingly, the discrepancy in the extent of inhibition observed between the clinical study and model simulations after acute goldenseal exposure may be due to an uncharacterized phytoconstituent in the complex mixture. The uncharacterized phytoconstituent could also contribute to the interaction after chronic goldenseal exposure such that the simulation overpredicted the inhibition potential of (−)-β-hydrastine. Testing every phytoconstituent in a natural product for enzyme or transporter modulation is not practical; thus, there are increased efforts to establish harmonized guidelines for studying these complex mixtures (Johnson et al., 2018; Paine et al., 2018; Kellogg et al., 2019; Cox et al., 2021). Second, there are no standardized methods to differentiate the effects of reversible inhibition from TDI in vivo. According to regulatory agencies, administration of multiple doses of a precipitant is necessary to adequately assess clinical TDI (https://www.ema.europa.eu/en/documents/scientific-guideline/guideline-investigation-drug-interactions-revision-1_en.pdf; https://www.fda.gov/media/134581/download; https://www.ema.europa.eu/en/ich-m12-drug-interaction-studies-scientific-guideline). By coadministering an inhibitor and the object drug, any observed interaction is attributed to reversible inhibition. Thus, claims of goldenseal precipitating interactions via TDI contradict observations after acute goldenseal exposure. A potential hypothesis is that TDI occurs more rapidly than conventional theory would suggest and that the 30 minutes between administration of goldenseal and midazolam was sufficient to produce clinical TDI (akin to the preincubation time required to observe TDI in vitro). Modeling and simulations suggest that maximal effects from TDI occur ~2 hours after exposure to the precipitant (Fig. 7D), showing that a single dose of a time-dependent inhibitor can produce pharmacokinetic drug interactions that persists for ~24 hours (Fig. 7F). In addition, the uniquely large dose of goldenseal could have additive effects via

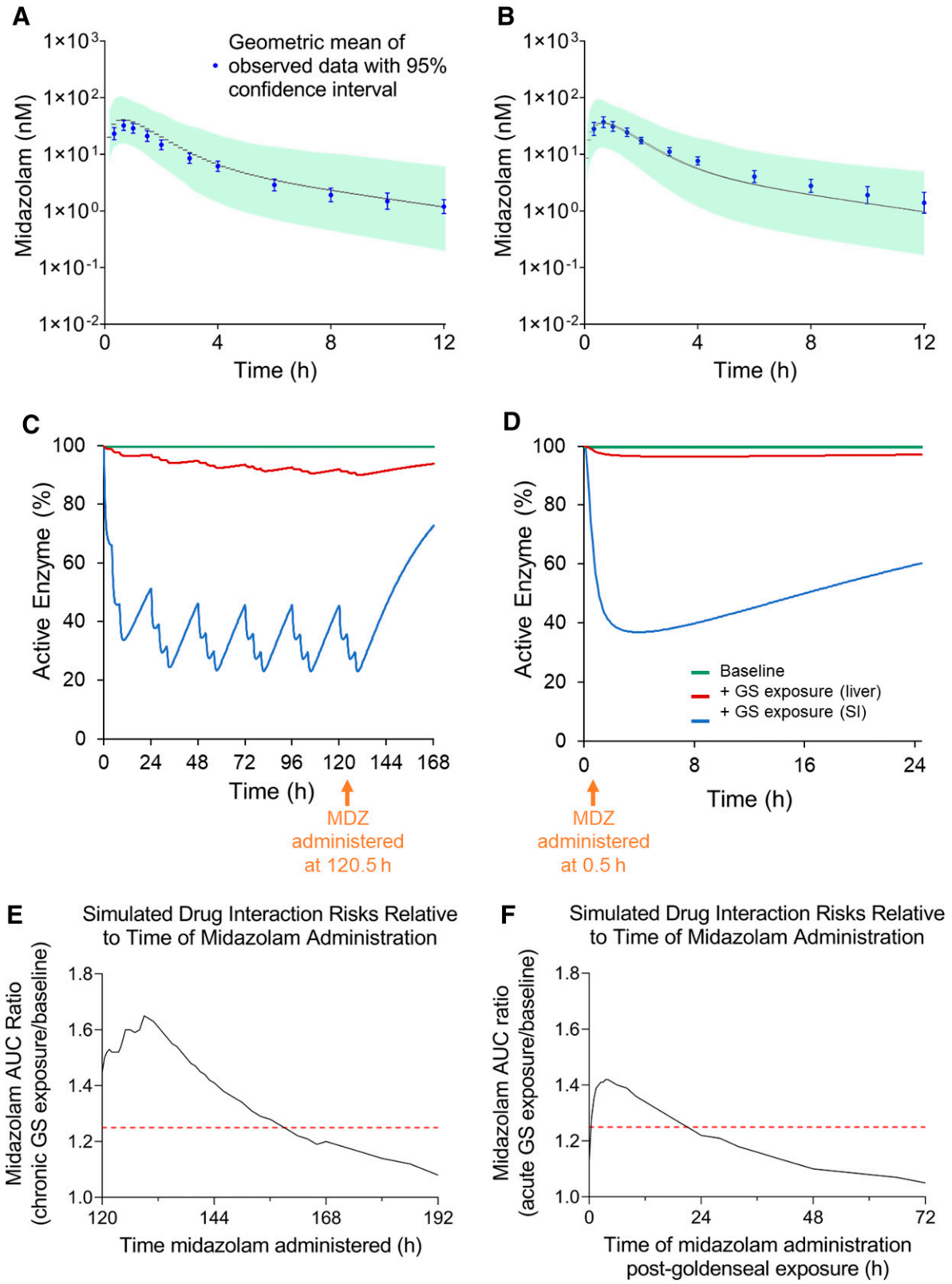

Fig. 7. Observed (blue dots) and simulated (gray lines) concentration-time profiles for an orally administered dose of midazolam (2.5 mg) after chronic (A) and acute (B) goldenseal exposure. Each observed data point represents the geometric mean of 16 and 8 participants for the chronic and acute goldenseal exposure groups, respectively. Green-shaded region denotes fifth and 95th percentiles for model simulations, whereas blue error bars denote the 90% confidence intervals for the observed data. Simulated time course of active CYP3A in the small intestine (SI) and liver before and after chronic (C) and acute (D) goldenseal (GS) exposure. Simulated drug interaction risk of the goldenseal-midazolam interaction with respect to time of midazolam administration after chronic (E) and acute (F) goldenseal exposure. Chronic exposure indicates multiple doses (1 g thrice daily × 6 days) of goldenseal, whereas acute exposure indicates a single dose (3 g) of goldenseal. Red dashes (E and F) indicate AUC ratio of 1.25, which represents the threshold for clinically relevant pharmacokinetic drug interactions.

TABLE 3
Predicted and observed changes in oral midazolam (2.5 mg) pharmacokinetics after chronic (1 g thrice daily for 6 days) or acute (a single 3-g dose) goldenseal administration
Data represent geometric means [90% confidence intervals]. Ratios denote the AUC_{0-12h} or C_{max} of midazolam in the presence to absence of goldenseal.

	Observed	Predicted	Predicted/Observed
	Midazolam Pharmacokinetics		
Chronic Goldenseal Exposure			
AUC_{0-12h} ratio	1.39 [1.30–1.48]	1.49 [1.46–1.53]	1.07
C_{max} ratio	1.31 [1.16–1.48]	1.43 [1.40–1.47]	1.10
Acute Goldenseal Exposure			
AUC_{0-12h} ratio	1.57 [1.39–1.77]	1.28 [1.27–1.30]	0.82
C_{max} ratio	1.40 [1.12–1.74]	1.26 [1.24–1.27]	0.90

reversible inhibition (Supplemental Table 5), as evidenced by the greater increase in midazolam AUC and C_{max} after acute compared with chronic goldenseal exposure. These observations indicate potential interplay between time-dependent and reversible inhibition. However, the acute goldenseal arm was exploratory and was not powered to detect pharmacokinetic changes between chronic and acute goldenseal exposure. Finally, the increased 1'-hydroxymidazolam AUC upon acute administration of goldenseal suggested activation, which is consistent with in vitro observations involving berberine. However, this feature was not incorporated into the PBPK model because an activation component is not currently available in the platform. Additionally, the increase in midazolam exposure after acute goldenseal administration may have directly led to the increase in 1'-hydroxymidazolam AUC and/or masked the effects of activation by berberine. Nevertheless, the clinical relevance of this modulatory effect remains equivocal.

In summary, an integrated approach involving data generated from in vitro assays, clinical studies, and PBPK modeling and simulation was used to identify the primary precipitant, mode of inhibition, and site of a pharmacokinetic natural product-drug interaction. The current work showed that TDI of intestinal CYP3A by (−)-β-hydrastine was the predominant mechanism underlying the goldenseal-midazolam interaction. Practically, TDI of CYP3A by goldenseal would have long-lasting effects, akin to grapefruit juice, even after a single dose. Thus, patients taking medications that are extensively metabolized by intestinal CYP3A (e.g., some statins, immunosuppressants, and calcium channel blockers) (Tanna et al., 2023) should be cautioned about consuming goldenseal. The integrated approach used in this study can be applied to other pharmacokinetic natural product-drug interactions to elucidate complex interactions between multiple phytoconstituents and varying mechanisms of enzyme inhibition.

Acknowledgments

The authors thank Judy Griffin for her expert nursing skills and Deena Hadi for her assistance with clinical study logistics. M.F.P. dedicates this article to David P. Paine. Certara UK Limited (Simcyp Division) granted access to the Simcyp Simulator through a sponsored academic license (subject to conditions).

Data Availability

The authors declare that all of the data supporting the findings of this study are available within the paper and the Supplemental Material and/or are openly available in the NaPDI Center Database (https://repo.napdi.org/).

Authorship Contributions

Participated in research design: Nguyen, Tian, Tanna, Rettie, Thummel, Paine.

Conducted experiments: Nguyen, Tian.

Contributed new reagents or analytic tools: Arian, Calamia.

Performed data analysis: Nguyen, Tian.

Wrote or contributed to the writing of the manuscript: Nguyen, Tian, Tanna, Arian, Paine.

References

Adiwidjaja J, Boddy AV, and McLachlan AJ (2022) Physiologically based pharmacokinetic model predictions of natural product-drug interactions between goldenseal, berberine, imatinib and bosutinib. *Eur J Clin Pharmacol* **78**:597–611.

Brantley SJ, Graf TN, Oberlies NH, and Paine MF (2013) A systematic approach to evaluate herb-drug interaction mechanisms: investigation of milk thistle extracts and eight isolated constituents as CYP3A inhibitors. *Drug Metab Dispos* **41**: 1662–1670.

Chatterjee P and Franklin MR (2003) Human cytochrome p450 inhibition and metabolic-intermediate complex formation by goldenseal extract and its methylenedioxyphenyl components. *Drug Metab Dispos* **31**:1391–1397.

Chiba M, Hensleigh M, and Lin JH (1997) Hepatic and intestinal metabolism of indinavir, an HIV protease inhibitor, in rat and human microsomes. Major role of CYP3A. *Biochem Pharmacol* **53**:1187–1195.

Cox EJ, Tian D-D, Clarke JD, Rettie AE, Unadkat JD, Thummel KE, McCune JS, and Paine MF (2021) Modeling pharmacokinetic natural product-drug interactions for decision-making: a NaPDI Center recommended approach. *Pharmacol Rev* **73**:847–859.

Guo Y, Chen Y, Tan Z-R, Klaassen CD, and Zhou H-H (2012) Repeated administration of berberine inhibits cytochromes P450 in humans. *Eur J Clin Pharmacol* **68**:213–217.

Gurley BJ, Gardner SF, Hubbard MA, Williams DK, Gentry WB, Khan IA, and Shah A (2005) In vivo effects of goldenseal, kava kava, black cohosh, and valerian on human cytochrome P450 1A2, 2D6, 2E1, and 3A4/5 phenotypes. *Clin Pharmacol Ther* **77**:415–426.

Gurley BJ, Swain A, Hubbard MA, Hartsfield F, Thaden J, Williams DK, Gentry WB, and Tong Y (2008) Supplementation with goldenseal (Hydrastis canadensis), but not kava kava (Piper methysticum), inhibits human CYP3A activity in vivo. *Clin Pharmacol Ther* **83**:61–69.

Hobbs C (1990) Golden seal in early American medical botany. *Pharm Hist* **32**:79–82.

Hubatsch I, Ragnarsson EGE, and Artursson P (2007) Determination of drug permeability and prediction of drug absorption in Caco-2 monolayers. *Nat Protoc* **2**:2111–2119.

Jamei M, Marciniak S, Edwards D, Wragg K, Feng K, Barnett A, and Rostami-Hodjegan A (2013) The Simcyp population based simulator: architecture, implementation, and quality assurance. *In Silico Pharmacol* **1**:9.

Jamei M, Marciniak S, Feng K, Barnett A, Tucker G, and Rostami-Hodjegan A (2009) The Simcyp population-based ADME simulator. *Expert Opin Drug Metab Toxicol* **5**:211–223.

Johnson EJ, González-Peréz V, Tian D-D, Lin YS, Unadkat JD, Rettie AE, Shen DD, McCune JS, and Paine MF (2018) Selection of priority natural products for evaluation as potential precipitants of natural product-drug interactions: a NaPDI Center recommended approach. *Drug Metab Dispos* **46**:1046–1052.

Kalgutkar AS, Obach RS, and Maurer TS (2007) Mechanism-based inactivation of cytochrome P450 enzymes: chemical mechanisms, structure-activity relationships and relationship to clinical drug-drug interactions and idiosyncratic adverse drug reactions. *Curr Drug Metab* **8**:407–447.

Kellogg JJ, Kvalheim OM, and Cech NB (2020) Composite score analysis for unsupervised comparison and network visualization of metabolomics data. *Anal Chim Acta* **1095**:38–47.

Kellogg JJ, Paine MF, McCune JS, Oberlies NH, and Cech NB (2019) Selection and characterization of botanical natural products for research studies: a NaPDI center recommended approach. *Nat Prod Rep* **36**:1196–1221.

Kronbach T, Mathys D, Umeno M, Gonzalez FJ, and Meyer UA (1989) Oxidation of midazolam and triazolam by human liver cytochrome P450IIIA4. *Mol Pharmacol* **36**:89–96.

Lalovic B, Phillips B, Risler LL, Howald W, and Shen DD (2004) Quantitative contribution of CYP2D6 and CYP3A to oxycodone metabolism in human liver and intestinal microsomes. *Drug Metab Dispos* **32**:447–454.

Lin YS, Dowling ALS, Quigley SD, Farin FM, Zhang J, Lamba J, Schuetz EG, and Thummel KE (2002) Co-regulation of CYP3A4 and CYP3A5 and contribution to hepatic and intestinal midazolam metabolism. *Mol Pharmacol* **62**:162–172.

McDonald MG, Tian D-D, Thummel KE, Paine MF, and Rettie AE (2020) Modulation of major human liver microsomal cytochromes P450 by component alkaloids of goldenseal: time-dependent inhibition and allosteric effects. *Drug Metab Dispos* **48**: 1018–1027.

Nguyen JT, Tian D-D, Tanna RS, Hadi DL, Bansal S, Calamia JC, Arian CM, Shireman LM, Molnár B, Horváth M, et al. (2021) Assessing transporter-mediated natural product-drug interactions via in vitro-in vivo extrapolation: clinical evaluation with a probe cocktail. *Clin Pharmacol Ther* **109**:1342–1352.

Obach RS, Walsky RL, and Venkatakrishnan K (2007) Mechanism-based inactivation of human cytochrome p450 enzymes and the prediction of drug-drug interactions. *Drug Metab Dispos* **35**:246–255.

Paine MF, Shen DD, Kunze KL, Perkins JD, Marsh CL, McVicar JP, Barr DM, Gillies BS, and Thummel KE (1996) First-pass metabolism of midazolam by the human intestine. *Clin Pharmacol Ther* **60**:14–24.

Paine MF, Shen DD, and McCune JS (2018) Recommended approaches for pharmacokinetic natural product-drug interaction research: a NaPDI Center commentary. *Drug Metab Dispos* **46**:1041–1045.

Pathak SM, Ruff A, Kostewicz ES, Patel N, Turner DB, and Jamei M (2017) Model-based analysis of biopharmaceutic experiments to improve mechanistic oral absorption modeling: an integrated in vitro in vivo extrapolation perspective using ketoconazole as a model drug. *Mol Pharm* **14**:4305–4320.

Safari D, DeMarco EC, Scanlon L, and Grossberg GT (2022) Over-the-counter remedies in older adults: patterns of use, potential pitfalls, and proposed solutions. *Clin Geriatr Med* **38**:99–118.

Sager JE, Yu J, Ragueneau-Majlessi I, and Isoherranen N (2015) Physiologically based pharmacokinetic (PBPK) modeling and simulation approaches: a systematic review of published models, applications, and model verification. *Drug Metab Dispos* **43**:1823–1837.

Sandhu RS, Prescilla RP, Simonelli TM, and Edwards DJ (2003) Influence of goldenseal root on the pharmacokinetics of indinavir. *J Clin Pharmacol* **43**:1283–1288.

Tanna RS, Nguyen JT, Hadi DL, Layton ME, White JR, Cech NB, Oberlies NH, Rettie AE, Thummel KE, and Paine MF (2023) Clinical assessment of the drug interaction potential of the psychotropic natural product kratom. *Clin Pharmacol Ther* **113**:1315–1325

Tanna RS, Tian D-D, Cech NB, Oberlies NH, Rettie AE, Thummel KE, and Paine MF (2021) Refined prediction of pharmacokinetic kratom-drug interactions: time-dependent inhibition considerations. *J Pharmacol Exp Ther* **376**:64–73.

Thummel KE, O'Shea D, Paine MF, Shen DD, Kunze KL, Perkins JD, and Wilkinson GR (1996) Oral first-pass elimination of midazolam involves both gastrointestinal and hepatic CYP3A-mediated metabolism. *Clin Pharmacol Ther* **59**:491–502.

Tian D-D, Leonowens C, Cox EJ, González-Pérez V, Frederick KS, Scarlett YV, Fisher MB, and Paine MF (2019) Indinavir increases midazolam *N*-glucuronidation in humans: identification of an alternate CYP3A inhibitor using an in vitro to in vivo approach. *Drug Metab Dispos* **47**:724–731.

Wallace ED, Todd DA, Harnly JM, Cech NB, and Kellogg JJ (2020) Identification of adulteration in botanical samples with untargeted metabolomics. *Anal Bioanal Chem* **412**:4273–4286.

Yamada M, Inoue S-I, Sugiyama D, Nishiya Y, Ishizuka T, Watanabe A, Watanabe K, Yamashita S, and Watanabe N (2020) Critical impact of drug-drug interactions via intestinal CYP3A in the risk assessment of weak perpetrators using physiologically based pharmacokinetic models. *Drug Metab Dispos* **48**:288–296.

Address correspondence to: Dr. Mary F. Paine, College of Pharmacy and Pharmaceutical Sciences, Washington State University, 412 East Spokane Falls Boulevard, Spokane, WA 99210. E-mail: mary.paine@wsu.edu

Supplemental Information

Titles: An Integrative Approach to Elucidate Mechanisms Underlying the Pharmacokinetic Goldenseal-Midazolam Interaction: Application of In Vitro Assays and Physiologically Based Pharmacokinetic Models to Understand Clinical Observations

Authors: James T. Nguyen, Dan-Dan Tian, Rakshit S. Tanna, Christopher M. Arian, Justina C. Calamia, Allan E. Rettie, Kenneth E. Thummel, Mary F. Paine

Journal: Journal of Pharmacology and Experimental Therapeutics

Manuscript Number: JPET-AR-2023-001681

Supplemental Methods.

Supplemental Table 1. Analytical methods for in vitro and clinical samples.

Supplemental Table 2. Physiochemical chemical properties and kinetic parameter inputs for berberine and (–)-β-hydrastine in Simcyp™.

Supplemental Table 3. Demographics of healthy participants in the clinical study.

Supplemental Table 4. Pharmacokinetics of midazolam (2.5 mg) after oral administration of midazolam alone and after chronic goldenseal exposure (1 g thrice daily for 6 days) for the 8 participants who completed all three arms of the study. Data represent geometric means [90% confidence intervals].

Supplemental Table 5. Comparison between observed and model simulated oral midazolam (2.5 mg) pharmacokinetics. Data represent geometric means [90% confidence intervals].

Supplemental Fig. 1. Inhibition of midazolam 1'-hydroxylation by extracts prepared from the goldenseal product administered in the clinical study. Extracts were preincubated in potassium phosphate buffer containing human liver microsomes (0.25 mg/mL) with and without NADPH for 30 minutes at 37°C. Thereafter, the solution was added to a secondary mixture containing midazolam (2 μM) and incubated for an additional 5 minutes prior to quenching with ice-cold 15% aqueous $ZnSO_4$ containing 1'-hydroxymidazolam (10 pM) as internal standard.

Supplemental Methods

Simcyp Population Based Simulator Inputs
Simcyp Version 22 (10/12/2022)

	Substrate	Inhibitor 1	Inhibitor 2
Compound	Midazolam	Hydrastine	Berberine
Mol Wt (g/mol)	325.80	383.39	336.37
log P	3.53	2.61	-1.2
Compound Type		Monoprotic Base	
pKa 1	6.00	6.16	14
pKa 2	n/a	n/a	n/a
B/P	0.60	1.00	1.00
Haematocrit	45.00	45.00	45
fu,p	0.03	0.06	0.59

Input Parameters	
Workspace	
Substrate	Midazolam
Inhibitor 1	Hydrastine
Inhibitor 2	Berberine
Simulation Mode	PKPD Profiles

	Substrate	Inhibitor 1	Inhibitor 2
GI Absorption Mo	1st order	ADAM	1st order
GI Permeability A	n/a	n/a	n/a
GI Peff,man	Regional	Regional	Regional
Distribution Model	Minimal PBPK	Full PBPK Model	Minimal PBPK
Vss (L/kg)	0.880	n/a	n/a
Vss	n/a	Predicted	Predicted
Prediction Method	Entered	Method 2	Method 2
Clearance Type	Enzyme Kinetic	In Vivo Clearance	

Trial Design	
Use Pop Representative	No
Population Size	160.000
Number of Trials	10.000
No of Subjects per Trial	16.000
Population name	Healthy adults
Minimum Age (years)	23.000
Maximum Age (years)	42.000
Propn. of Females	0.500
Fix Individual Trial Design	No
Prandial State	Fasted
Fluid intake with dose (mL)	250.000
Fluid intake with dose CV (%)	30.000
PKPD Parameters	Off
PKPD Profiles	On
Start Day/Time	Day 1, 06:00
End Day/Time	Day 8, 06:30
Study Duration (h)	168.500

	Substrate	Inhibitor 1	Inhibitor 2
Prandial State	Fasted	n/a	n/a
Route	Oral	Custom	Custom
Dose Units	mg	n/a	n/a
Dose	2.500	n/a	n/a
Start Day/Time	Day 6, 06:30	n/a	n/a
Dosing Regimen	Single Dose	n/a	n/a

Hydrastine Dosing

Day	Time	Offset (h)	Dose	Dose Units	Route
1,2,3,4,5,6	6:00:00	0	25.400	mg	Oral
1,2,3,4,5,6	10:00:00	4	25.400	mg	Oral
1,2,3,4,5,6	14:00:00	8	25.400	mg	Oral

Berberine Dosing

Day	Time	Offset (h)	Dose	Dose Units	Route
1,2,3,4,5,6	6:00:00	0	29.800	mg	Oral
1,2,3,4,5,6	10:00:00	4	25.400	mg	Oral
1,2,3,4,5,6	14:00:00	8	25.400	mg	Oral

Compound	Midazolam
Molecule Type	Small Molecule
Route	Oral
Dose Units	mg
Dose	2.500
Start Day	6.000
Start Time	6h30m
Dosing Regimen	Single Dose
PhysChem and Blood Binding	
Mol Weight (g/mol)	325.800
log P	3.530
Compound Type	Monoprotic Base
pKa 1	6.000
Extended Clearance	Class 2 - Metabolism
BP input type	User
B/P	0.603
Haematocrit	45.000
fu Input	User
fu	0.032
Reference Binding	HSA
Protein Reference	45.000
% Bound to Lipoprotein	0.000
% Bound to Lipoprotein	0.000
Absorption	
Absorption Model	1st order
Input type	User
fa	1.000
CV fa (%)	30.000
ka (1/h)	3.000
CV ka (%)	30.000
lag time (h)	0.000
CV lag time (%)	30.000
fu(Gut) input type	User
fu(Gut)	1.000
Q(Gut) input type	Predicted
Peff,man Type	n/a
Peff,man Cap (10	12.000
Permeability Assay	PCaco-2
Apical pH : Basola	7.4 : 7.4
Activity	Passive & Active
PCaco-2(10E-06 c	213.000
Reference Compou	Multiple
Reference Compou	0.000
Scalar	0.290

Compound	Hydrastine
Molecule Type	Small Molecule
Route	Oral
PhysChem and Blood Binding	
Mol Weight (g/mol)	383.390
log P	2.610
Compound Type	Monoprotic Base
pKa 1	6.160
Extended Clearance	Class 2 - Metabolism
BP input type	User
B/P	1.000
Haematocrit	45.000
fu Input	User
fu	0.060
Reference Binding	HSA
Protein Reference	45.000
% Bound to Lipoprotein	0.000
% Bound to Lipoprotein	0.000
Absorption	
Absorption Model	ADAM
Use UBL fluid	No
fu(Gut) input type	User
fu(Gut)	1.000
Peff,man Type	Global
Peff,man Cap	12.000
Permeability Assay	PCaco-2
Apical pH : Basola	6.5 : 7.4
Activity	Passive & Active
PCaco-2(10E-06 c	9.720
Reference Compou	Midazolam
Reference Compou	13.200
Scalar	5.705
Degradation Rate	0.000
Degradation Rate	0.000
Degradation Rate	0.000
Degradation Rate	0.000
Degradation Rate	0.000
Degradation Rate	0.000
Degradation Rate	0.000
Input Form	Solid Formulation
Dual Solid Stage	No
Formulation	Immediate Release (IR)

Compound	Berberine
Molecule Type	Small Molecule
Route	Oral
PhysChem and Blood Binding	
Mol Weight (g/mol)	336.370
log P	-1.200
Compound Type	Monoprotic Base
pKa 1	14.000
Extended Clearance	Class 4 - Renal
BP input type	User
B/P	1.000
Haematocrit	45.000
fu Input	User
fu	0.590
Reference Binding	HSA
Protein Reference	45.000
% Bound to Lipoprotein	0.000
% Bound to Lipoprotein	0.000
Absorption	
Absorption Model	1st order
Input type	Predicted
fa	Predicted
ka (1/h)	Predicted
lag time (h)	0.000
CV lag time (%)	30.000
fu(Gut) input type	User
fu(Gut)	1.000
Q(Gut) input type	Predicted
Peff,man input type	Predicted
Peff,man Cap (10-	12.000
Permeability Assay	PCaco-2
Apical pH : Basola	6.5 : 7.4
Activity	Passive & Active
PCaco-2(10E-06 c	0.185
Reference Compou	Atenolol
Reference Compou	0.156
Scalar	1.218
Distribution	
Distribution Model	Minimal PBPK Model
SAC kin (1/h)	0.000
SAC kout (1/h)	0.000
Volume [Vsac] (L/k	7.32E-04

Distribution	
Distribution Mode	Minimal PBPK Model
SAC kin (1/h)	0.200
SAC kout (1/h)	0.250
Volume [Vsac] (L	2.30E-01
Vss input type	User
Vss (L/kg)	0.880
CV Vss (%)	30.000
Liver input type	User
Liver Kp	1.000

Elimination	
Clearance Type	Enzyme Kinetics
FI Correction	Not used
PLR Correction	Not Used
In vitro metabolic	Recombinant
Pathway	1-OH
Enzyme	CYP3A4
Vmax (pmol/min/	5.230
Km (µM)	2.160
fu mic	1.000
Pathway	1-OH
Enzyme	CYP3A5
Vmax (pmol/min/	19.700
Km (µM)	4.160
fu mic	1.000
Pathway	4-OH
Enzyme	CYP3A4
Vmax (pmol/min/	5.200
Km (µM)	31.800
fu mic	1.000
Pathway	4-OH
Enzyme	CYP3A5
Vmax (pmol/min/	4.030
Km (µM)	38.400
fu mic	1.000
In vitro metabolic system	HLM
Pathway	Pathway 3
Enzyme	UGT1A4

Define Disinte	Not activated
Dissolution Ty	Dissolution
Dissolution Inp	Discrete
Allow Non-mo	No
Interpolation A	Linear
Dissolution Profile (All)	
Fasted Time (	0.000
Fasted Dissol	0.000
Fasted CV (%	0.000
Fasted Time (	0.083
Fasted Dissol	16.000
Fasted CV (%	7.000
Fasted Time (	0.166
Fasted Dissol	35.000
Fasted CV (%	25.000
Fasted Time (	0.250
Fasted Dissol	69.000
Fasted CV (%	13.000
Fasted Time (	0.333
Fasted Dissol	83.000
Fasted CV (%	12.000
Fasted Time (	0.416
Fasted Dissol	87.000
Fasted CV (%	11.000
Fasted Time (	0.500
Fasted Dissol	89.000
Fasted CV (%	9.000
Fasted Time (	1.000
Fasted Dissol	100.000
Fasted CV (%	7.000
Fasted Time (	2.000
Fasted Dissol	100.000
Fasted CV (%	11.000
Absorption Sc	SI Global
Absorption Sc	1.000
Absorption Sc	1.000
Basolateral Pe	SI Global
Basolateral Pe	1.000
Basolateral Pe	1.000
Segregated tra	Not activated

Distribution	
Distribution Model	Full PBPK Model
Replacement	No
Organ Replac	n/a
User-defined A	No
Type	n/a

Vss input type	Predicted
Prediction Method	Method 2
Concentration-dep	No
log Po:w	-1.200
$Ka_{,AP}$ input type	Predicted
logP vo:w input typ	Predicted
logP vo:w Predictic	Hansch
logP vo:w Hansch	1.115
logP vo:w Hansch	-1.350
Compound Type	Monoprotic Base
pKa 1	14.000
Adipose input type	Predicted
Bone input type	Predicted
Brain input type	Predicted
Gut input type	Predicted
Heart input type	Predicted
Kidney input type	Predicted
Liver input type	Predicted
Lung input type	Predicted
Muscle input type	Predicted
Skin input type	Predicted
Spleen input type	Predicted
Pancreas input typ	Predicted
Kp Scalar	1.000
Smoothing Functio	Off
Lipid Binding Scala	1.000
Use Pvo:w for Neu	No

Elimination	
Clearance Type	In Vivo Clearance
CL (po) (L/h)	32574.000
CV CL (po) (%)	69.000
Active Hepatic Sca	1.000
CL R (L/h)	0.000
CYPs and/or UGTs	Interaction
Enzyme	CYP3A4
Ki (µM)	250.000
fu mic	0.650
MBI Kapp (µM)	14.800
MBI Kinact (1/h)	1.140
MBI fu mic	0.650
MIA (pmol/mg microsomal protein)	251.121
Consider Competit	No

Vmax (pmol/min/	445.000
Km (µM)	40.300
fu mic	1.000
Feed formed renal metabolite into kidney	No
Use Allelic variants for Enzyme 1	No
Enzyme	CYP2C9
Use Allelic variants for Enzyme 2	No
Enzyme	CYP1A2
Gut Lumen metabolism	in-active
Ontogeny Profile	No Profile Used
Ontogeny Profile	No Profile Used
Ontogeny Profile	No Profile Used
Biliary CLint (Hep	0.000
CV Biliary CLint (	30.000
Ontogeny Profile	No Profile Used
Active enterohep	No
Active Hepatic S	1.000
CL R (L/h)	0.085
Organ/Tissue	Tumour
Tumour Permeab	Off

Vss input type	Predicted
Prediction Met	Method 2
Concentration	No
log Po:w	2.610
logP vo:w inpu	Predicted
logP vo:w Pre	Hansch
logP vo:w Har	1.115
logP vo:w Har	-1.350
Compound Ty	Monoprotic Base
pKa 1	6.160
Adipose input	Predicted
Bone input typ	Predicted
Brain input typ	Predicted
Gut input type	Predicted
Heart input typ	Predicted
Kidney input ty	Predicted
Liver input typ	Predicted
Lung input typ	Predicted
Muscle input t	Predicted
Skin input type	Predicted
Spleen input ty	Predicted
Pancreas inpu	Predicted
Kp Scalar	1.000
Smoothing Fu	Off
Lipid Binding S	1.000
Use Pvo:w for	No

Elimination

Clearance Type	In Vivo Clearance
CL (po) (L/h)	158.000
CV CL (po) (%	96.000
Active Hepatic	1.000
CL R (L/h)	0.250
Enzyme	CYP3A4
Ki (µM)	22.900
fu mic	0.930
MBI Kapp (µM	8.480
MBI Kinact (1/	2.460
MBI fu mic	0.930
MIA (pmol/mg	251.121
Enzyme	CYP3A5
Ki (µM)	22.900
fu mic	0.930
MBI Kapp (µM	8.480
MBI Kinact (1/	2.460
MBI fu mic	0.930
MIA (pmol/mg	220.935

Co-administration (	Default
Co-administration (	Default

Transporters Interaction

Organ/Tissue	Gut
Transporter	SLC22A1 (OCT1)
Ki (µM)	9.500
fuinc (Ki)	1.000
Organ/Tissue	Tumour
Tumour Permeabil	Off

Supplemental Table 1. Analytical methods for *in vitro* and clinical samples.

Analyte (*in vitro* samples)	**Midazolam**	**Midazolam metabolites**	**Berberine**	**(–)-β-hydrastine**	**Atenolol**
Mass Spectrometry	SCIEX QTRAP® 6500 equipped with Shimadzu Nexera X2 UPLC				
LC column	Aquasil C18 (50 x 2.1 mm, 3 µm; Thermo Fisher Scientific Inc., Waltham, MA)				
Mobile phase	A: water + 0.1% formic acid B: methanol + 0.1% formic acid				
Mobile phase gradient % B (min)	10% methanol (0.4 min) → 60% methanol (1.0 min) → 95% methanol (2.0 min) → 95% methanol (3.0 min) → 10% methanol (3.1 min) → 10% methanol (4.0 min)		5% methanol (0.4 min) → 95% methanol (1.5 min) → 95% methanol (2.0 min) → 5% methanol (2.1 min) → 5% methanol (3.0 min)		
Ionization mode	Multiple reaction monitoring: positive mode				
Internal standard (IS)	Alprazolam				
Transition (*m/z*)	326 → 291 309 → 205 (IS)	1'-OH: 342 → 203 4-OH: 342 → 325 309 → 205 (IS)	336 → 320 309 → 205 (IS)	384 → 323 309 → 205 (IS)	267 → 190 309 → 205 (IS)

Analyte (clinical samples)	**Midazolam**	**Midazolam metabolites**	**Berberine**	**(–)-β-hydrastine**
Mass Spectrometry	Agilent 6410 Triple Quadrupole equipped with HPLC 1290 system		Waters Xevo TQ-S-2 equipped with I-Class Acquity UPLC	
LC column	Phenomenex Synergi polar RP, 2x 250 mm, 4 µm		Zorbax, Extend-C18 1.8 micron, 2.1x 50 mm	
Mobile phase	A: water + 0.1% formic acid B: methanol + 0.1% formic acid		A: water + 0.1% formic acid B: methanol + 0.1% formic acid	
Mobile phase gradient	35% methanol (1 min) → 60% methanol (15.0 min) → 60% methanol (17.0 min) → 35% methanol (17.1 min)		5% methanol (0.0 min) → 100% methanol (4.0 min) → 100% methanol (6.0 min) → 95% methanol (6.1 min)	
Ionization mode	Multiple reaction monitoring: positive mode			
Internal standard (IS)	midazolam-*d*4	1'-hydroxymidazolam-*d*4 4-hydroxymidazolam-*d*5	berberine-*d*6	
Transition (*m/z*)	326 → 291 330 → 291 (IS)	1'-OH: 342 → 291 346 → 168 (IS) 1'-*O*-gluc: 518 → 324 4-OH: 342 → 297 347 → 300 (IS) 4-*O*-gluc: 518 → 342 *N*-gluc: 502 → 326	336 → 320 342 → 294 (IS)	384 → 323 342 → 294 (IS)

Supplemental Table 2. Physiochemical chemical properties and kinetic parameter inputs for berberine and (–)-β-hydrastine in Simcyp™.

Berberine (29.8 mg/g goldenseal product)		
Physicochemical Properties and Blood Binding		
MW (g/mol)	336.37	
LogP	-1.2	Spinozzi *et al.* J Nat Prod. 2014, 77(4):766-72.
pKa	monoprotic base 14	Observed pKa is 15 but the maximum input is 14 in Simcyp™; Spinozzi *et al.* J Nat Prod. 2014, 77(4):766-72.
B/P	1	Assumed
$f_{u,p}$	0.59	In-house measurement via equilibrium dialysis
Plasma binding	HSA	Assumed
Absorption – 1st order absorption model		
P_{eff} (10-4 cm/s)	0.167	Predicted using P_{app} within Simcyp™
P_{app} (10^{-6} cm/s)	0.185 (pH 6.5 : 7.4)	In-house measurement (atenolol scaler: 0.156)
$f_{u,gut}$	1	Assumed
Q_{gut} (L/h)	1.39	Predicted within Simcyp™.
Distribution – Minimal PBPK model		The single adjusting compartment was deactivated to minimize model complexity as recommended in common practices.
V_{ss} (L/kg)	78.6	Predicted using Method 2
Elimination - In vivo clearance		
Cl/F(L/h)	32574	Calculated as Dose/AUC and weighted based on sample size from two independent clinical studies; Gupta *et al*. Planta Med. 2010. 76- P110.; Hua *et al*. J Pharm Biomed Anal. 2007. 44(4):931-7.
CV (%)	60	Calculated using reported mean AUC and SD; Gupta *et al*. Planta Med. 2010. 76- P110.; Hua *et al*. J Pharm Biomed Anal. 2007. 44(4):931-7.
CL_R(L/h)	0	Assumed
Interaction – CYP3A4		
Reversible inhibition		
K_i (μM)	250	Calculated as K_i=IC_{50}/2 when substrate concentration is ~K_m; Measured in HLMs; McDonald *et al*. Drug Metab Dispos. 2020, 48(10):1018-1027.
$f_{u,mic}$	0.65	Corrected[a] value of in-house $f_{u,mic}$ (0.90), which was determined using equilibrium dialysis at HLM concentrations of 0.05 mg/mL and adjusted to inhibition assay conditions of 0.25 mg/mL.
Time dependent inhibition		
K_I (μM)	14.8	Measured in HLMs; McDonald *et al*. Drug Metab Dispos. 2020, 48(10):1018-1027.
K_{inact} (h^{-1})	1.14	
$f_{u,mic}$	0.65	Corrected[a] value of in-house $f_{u,mic}$ (0.90), which was determined using equilibrium dialysis at HLM concentrations of 0.05 mg/mL and adjusted to inhibition assay conditions of 0.25 mg/mL.

(–)-β-hydrastine (25.4 mg/g goldenseal product)		
Physicochemical Properties and Blood Binding		
MW (g/mol)	383.39	
LogP	2.61	ADMET Predictor™ (version 10.3)
pKa	monoprotic base 6.16	ADMET Predictor™ (version 10.3)
B/P	1	Assumed
$f_{u,p}$	0.06	In house measurement via equilibrium dialysis
Plasma binding	HSA	Assumed
Absorption – ADAM model		
Formulation	Immediate Release	Dissolution profile integrated into model development.
P_{eff} (10^{-4} cm/s)	7.07	Predicted using P_{app} within Simcyp™
P_{app} (10^{-6} cm/s)	9.72 (pH 6.5 : 7.4)	In-house measurement (midazolam scaler: 13.2)
$f_{u,gut}$	1	Assumed
Q_{gut} (L/h)	16.9	Predicted using P_{eff} within Simcyp™
Distribution – Full PBPK model		
V_{ss} (L/kg)	1.01	Predicted using Method 2
Elimination – In vivo clearance		
Cl/F(L/h)	158	Estimated using (–)-β-hydrastine PK after oral administration (Dose/AUC); Gupta *et a*l. Drug Metab Dispos. 2015,43:545-552.
CV (%)	96	
CL_R (L/h)	0.25	Calculated based on previous published urinary excretion and AUC; Gupta *et a*l. Drug Metab Dispos. 2015,43:545-552.
Interaction – CYP3A4 and CYP3A5		
Reversible inhibition		
K_i (µM)	22.9	Calculated as $K_i=IC_{50}/2$ when substrate concentration is ~K_m; Measured in HIMs; Tanna *et al*. FASEB J. 33(S1):814.14.
$f_{u,mic}$	0.93	In-house experimental $f_{u,mic}$ determined using equilibrium dialysis with HIM concentration of 0.05 mg/mL.
Time dependent inhibition		
K_I (µM)	8.48	Measured in HIMs; No difference in TDI toward CYP3A4 and CYP3A5; identical K_I and k_{inact} values were used for both isoforms
k_{inact} (h^{-1})	2.46	
$f_{u,mic}$	0.93	In-house experimental $f_{u,mic}$ determined using equilibrium dialysis with HIM concentration of 0.05 mg/mL.

MW, molecular weight; LogP, lipophilicity; pK_a, log ionization constants; B/P, equilibrium blood-to-plasma concentration ratio; $f_{u,p}$, fraction unbound in plasma; P_{eff}, effective permeability; P_{app}, apparent permeability; $f_{u,gut}$, fraction unbound in gut; Q_{gut}, model to estimate gut first pass metabolism; V_{ss}, steady-state volume of distribution; Cl/F, oral clearance; CL_R, renal clearance; K_i, reversible inhibition constant; $f_{u,mic}$, fraction unbound in microsomal incubation; K_I, time-dependent inhibition constant; k_{inact}, maximum rate of inactivation; HIMs, human intestinal microsomes; HLMs, human liver microsomes.

[a] Austin *et al*. Drug Metab Dispos. 2002, 30(12):1497-1503.

Supplemental Table 3. Demographics of healthy participants in the clinical study.

	Control and chronic goldenseal exposure		**Acute goldenseal exposure**	
	Males (n=8)	Females (n=8)	Males (n=4)	Females (n=4)
Age (years; Median, range)	27 (23 - 42)	27 (23 - 35)	32.5 (26 - 42)	27.5 (23 - 35)
Weight (kg; Mean ± SD)	88.7 ± 18.1	67.9 ± 9.6	93.2 ± 18.9	63.6 ± 12.2
Self-identified race/ethnicity (n)				
Caucasian	7	6	4	3
Asian	1	2	0	1

Supplemental Table 4. Pharmacokinetics of midazolam (2.5 mg) after oral administration of midazolam alone and after chronic goldenseal exposure (1 g thrice daily for 6 days) for the 8 participants who completed all three arms of the study. Data represent geometric means [90% confidence intervals].

	Baseline	Chronic Exposure	Chronic/Baseline
Midazolam (MDZ)			
$AUC_{0\text{-}12h}$ (nM*h)	64.7 [48.8-85.9]	92.9 [68.5-126]	1.43 [1.25-1.64]
AUC_{inf} (nM*h)	69.5 [51.4-94.0]	104 [76.2-143]	1.50 [1.31-1.71]
$t_{1/2}$ (h)	3.71 [3.12-4.41]	4.66 [4.05-5.35]	1.25 [0.95-1.65]
C_{max} (nM)	26.8 [19.5-36.8]	36.2 [26.9-48.8]	1.35 [1.13-1.61]
t_{max} (h)[a]	0.67 [0.33-1.00]	0.67 [0.33-1.50]	N/A
Cl/F (L/h)	110 [81.9-149]	73.8 [54.0-101]	0.66 [0.58-0.76]
Cl_R (L/h)	0.05 [0.02-0.10]	0.06 [0.03-0.09]	1.21 [0.95-1.52]

$AUC_{0\text{-}12h}$, area under the plasma concentration versus time curve from 0-12 h; AUC_{inf}, area under the concentration versus time curve from 0 h to infinity; $t_{½}$, terminal half-life; C_{max}, maximum plasma concentration; t_{max}, time to reach C_{max}; Cl/F, apparent oral clearance; CL_R, renal clearance.

[a] Denotes median [range]

Supplemental Table 5. Comparison between observed and model simulated oral midazolam (2.5 mg) pharmacokinetics. Data represent geometric means [90% confidence intervals].

	Observed	Predicted	Predicted (TDI deactivated)	Predicted ((–)-β-hydrastine removed)	Predicted (IV midazolam)
Midazolam pharmacokinetics after chronic[a] goldenseal exposure					
$AUC_{0\text{-}12h}$ ratio	1.39 [1.30-1.48]	1.49 [1.46-1.53]	1.02 [1.02-1.02]	1.00 [1.00-1.00]	1.05 [1.05-1.06]
C_{max} ratio	1.31 [1.16-1.48]	1.43 [1.40-1.47]	1.02 [1.02-1.02]	1.00 [1.00-1.00]	1.00 [1.00-1.00]
Midazolam pharmacokinetics after acute[b] goldenseal exposure					
$AUC_{0\text{-}12h}$ ratio	1.57 [1.39-1.77]	1.28 [1.27-1.30]	1.05 [1.05-1.05]	1.00 [1.00-1.00]	1.01 [1.01-1.02]
C_{max} ratio	1.40 [1.12-1.74]	1.26 [1.24-1.27]	1.06 [1.06-1.06]	1.00 [1.00-1.00]	1.00 [1.00-1.00]
Midazolam pharmacokinetics after berberine 300 mg thrice daily x 14 days[c]					
$AUC_{0\text{-}12h}$ ratio	1.37 [1.12-1.67]	1.41 [1.38-1.43]	1.00 [1.00-1.00]		
C_{max} ratio	1.38 [1.07-1.77]	1.38 [1.36-1.41]	1.00 [1.00-1.00]		

Ratios determined as presence to absence of goldenseal.

[a] Goldenseal (1 g) was administered thrice daily x 6 days.

[b] A single dose of goldenseal (3 g) was administered.

[c] Guo *et al*. Eur J Clin Pharmacol. 2012, 68:213–7.

Supplemental Fig. 1. Inhibition of midazolam 1'-hydroxylation by extracts prepared from the goldenseal product administered in the clinical study. Extracts were preincubated in potassium phosphate buffer containing human liver microsomes (0.25 mg/mL) with and without NADPH for 30 minutes at 37°C. Thereafter, the solution was added to a secondary mixture containing midazolam (2 µM) and incubated for an additional 5 minutes prior to quenching with ice-cold 15% aqueous $ZnSO_4$ containing 1'-hydroxymidazolam (10 pM) as internal standard.

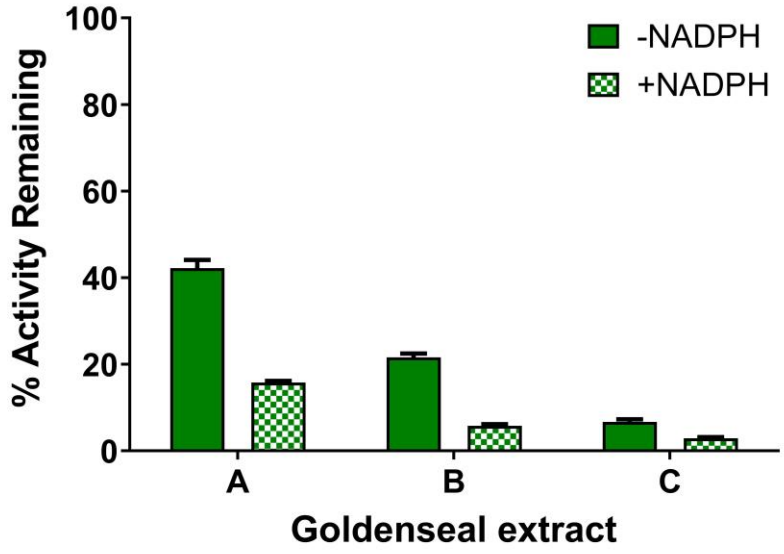

Concentrations of berberine and (–)-β-hydrastine in the goldenseal extract tested:

(A) berberine 2.68 µM; (–)-β-hydrastine 0.81 µM

(B) berberine 9.05 µM; (–)-β-hydrastine 2.72 µM

(C) berberine 26.8 µM; (–)-β-hydrastine 8.11 µM